Atmos. Chem. Phys. Discuss., 14, 13817–13867, 2014
www.atmos-chem-phys-discuss.net/14/13817/2014/
doi:10.5194/acpd-14-13817-2014

Atmospheric Chemistry and Physics
Open Access
Discussions

Seasonal variability of atmospheric nitrogen oxides and non-methane hydrocarbons at the GEOSummit station, Greenland

L. J. Kramer[1], D. Helmig[2], J. F. Burkhart[3,6], A. Stohl[3], S. Oltmans[4,5], and R. E. Honrath[1,†]

[1]Atmospheric Sciences Program/Dept. of Geological and Mining Engineering and Sciences, Michigan Technological University, Houghton, Michigan, USA
[2]Institute of Arctic and Alpine Research, University of Colorado, Boulder, CO, USA
[3]Norwegian Institute for Air Research (NILU), Kjeller, Norway
[4]NOAA Earth System Research Laboratory, Boulder, CO, USA
[5]CIRES, University of Colorado, Boulder, Colorado, USA
[6]Now at Department of Geosciences, University of Oslo, Norway
[†]deceased

Received: 1 May 2014 – Accepted: 8 May 2014 – Published: 27 May 2014

Correspondence to: L. J. Kramer (lkramer@mtu.edu)

Published by Copernicus Publications on behalf of the European Geosciences Union.

Abstract

Measurements of atmospheric NO_x ($NO_x = NO + NO_2$), peroxyacetyl nitrate (PAN), NO_y and non-methane hydrocarbons (NMHC) were taken at the GEOSummit Station, Greenland (72.34° N, 38.29° W, 3212 m.a.s.l) from July 2008 to July 2010. The data set represents the first year-round concurrent record of these compounds sampled at a high latitude Arctic site in the free troposphere. Here, the study focused on the seasonal variability of these important ozone (O_3) precursors in the Arctic free troposphere and the impact from transported anthropogenic and biomass burning emissions. Our analysis shows that PAN is the dominant NO_y species in all seasons at Summit, varying from 49 % to 78 %, however, we find that odd NO_y species (odd $NO_y = NO_y - PAN - NO_x$) contribute a large amount to the total NO_y speciation with monthly means of up to 95 pmol mol^{-1} in the winter and ~ 40 pmol mol^{-1} in the summer, and that the level of odd NO_y species at Summit during summer is greater than that of NO_x. We hypothesize that the source of this odd NO_y is most likely alkyl nitrates from transported pollution, and photochemically produced species such as HNO_3 and HONO.

FLEXPART retroplume analysis and tracers for anthropogenic and biomass burning emissions, were used to identify periods when the site was impacted by polluted air masses. Europe contributed the largest source of anthropogenic emissions during the winter and spring months, with up to 82 % of the simulated anthropogenic black carbon originating from this region between December 2009 and March 2010, whereas, North America was the primary source of biomass burning emissions. Polluted air masses were typically aged, with median transport times to the site from the source region of 11 days for anthropogenic events in winter, and 14 days for BB plumes. Overall we find that the transport of polluted air masses to the high altitude Arctic typically resulted in high variability in levels of O_3 and O_3 precursors. During winter, plumes originating from mid-latitude regions and transported in the lower troposphere to Summit often result in lower O_3 mole fractions than background levels. However, plumes

ACPD
14, 13817–13867, 2014

Seasonal variability of nitrogen oxides and NMHC at Summit

L. J. Kramer

transported at higher altitudes can result in positive enhancements in O_3 levels. It is therefore likely that the air masses transported in the mid-troposphere were mixed with air from stratospheric origin. Similar enhancements in O_3 and its precursors were also observed during periods when FLEXPART indicated that biomass burning emissions impacted Summit. The analysis of anthropogenic events over summer show that emissions of anthropogenic origin have a greater impact on O_3 and precursor levels at Summit than biomass burning sources during the measurement period, with enhancements above background levels of up to 16 $nmol\,mol^{-1}$ for O_3 and 237 $pmol\,mol^{-1}$ and 205 $pmol\,mol^{-1}$, 28 $pmol\,mol^{-1}$ and 1.0 $nmol\,mol^{-1}$ for NO_y, PAN, NO_x and ethane, respectively.

1 Introduction

The seasonality of ozone (O_3) and its precursors for photochemical production, such as NO_x ($NO_x = NO + NO_2$), peroxyacetyl nitrate (PAN) and non-methane hydrocarbons (NMHC), in the remote Arctic troposphere is governed by a combination of transport pathways, photochemistry and stratospheric influx (Klonecki et al., 2003; Stohl et al., 2006; Law and Stohl, 2007; Liang et al., 2011). Improving our knowledge on the seasonality of O_3 and its precursors and the relative importance of source regions and transport variability is essential as recent studies have suggested that tropospheric O_3 may have a large impact on radiative forcing and climate feedbacks in the Arctic region (Shindell et al., 2006; Shindell, 2007; Quinn et al., 2008).

Polluted air masses originating from anthropogenic and biomass burning sources in the mid-latitude regions can transport long-lived reservoir species of NO_x, such as PAN, and nitric acid (HNO_3) to the arctic region (Wofsy et al., 1992; Wespes et al., 2012), which may reform NO_x and result in enhanced levels far downwind from the emission sources (Beine et al., 1997; Walker et al., 2010). NMHC may also be transported in air masses from anthropogenic and biomass burning sources. The mole fractions of NMHC in the Arctic can vary greatly during the year due to seasonal variability

ACPD
14, 13817–13867, 2014

in emissions, transport pathway variability and the reaction with OH radicals (Jobson et al., 1994; Blake et al., 2003; Swanson et al., 2003).

Studies of pollution plumes with airborne, satellite- and ground-based observations and model simulations show that long-range transport from Europe and North America to the lower Arctic troposphere may constitute a large source of tropospheric O_3 and O_3 precursors, whereas at higher altitudes, pollution plumes transported from Asia become important (e.g. Klonecki et al., 2003; Law and Stohl, 2007; Shindell et al., 2008; Walker et al., 2012; Wespes et al., 2012). A large contribution to the seasonality of O_3 and O_3 precursors in the Arctic troposphere is due to variability in the location of the Arctic polar front (Klonecki et al., 2003; Stohl, 2006). During winter in the Northern Hemisphere, the polar front expands southward over North America, Europe and North Asia allowing direct transport of polluted air masses from sources within these latitudes to the Arctic. The Arctic polar front recedes in summer, reducing the impact of these pollution sources on the Arctic lower troposphere. However, it has been shown that the transport of emissions from biomass burning regions to the Arctic is possible during summer (Stohl, 2006) and that they can strongly impact the atmosphere above Summit Station in Greenland (Stohl et al., 2006). Results from a modeling study by Walker et al. (2012) using tagged emissions from the global chemical transport model GEOS-Chem show that during summer the primary emissions that impact the production of O_3 in the Arctic region were from high latitude regions, whereas, during the fall and winter periods, transport of emissions from mid-latitude regions in North America and Europe is possible.

A number of studies have discussed the seasonality of surface O_3 (Bottenheim et al., 1994; Beine et al., 1997; Monks, 2000; Browell et al., 2003; Helmig et al., 2007b; Walker et al., 2012), nitrogen oxides (Barrie and Bottenheim, 1991; Honrath and Jaffe, 1992; Bottenheim et al., 1994; Muthuramu et al., 1994; Beine et al., 1997; Solberg et al., 1997; Dibb et al., 1998; Munger et al., 1999; Beine and Krognes, 2000; Stroud et al., 2003; Thomas et al., 2011) and NMHC (Jobson et al., 1994; Blake et al., 2003; Klonecki et al., 2003; Swanson et al., 2003; Helmig et al., 2014a) in the Arctic region. However, due to the logistical difficulties in measuring at remote Arctic locations, the majority of seasonal studies have taken place at coastal sites in Northern Europe, Canada, and Alaska, or focused on the late spring/summer periods. Seasonal and interannual studies of nitrogen oxides in the remote Arctic free troposphere are largely missing. The high altitude Arctic has negligible impact from local pollution sources, and local production of NO_x from PAN decomposition is expected to be small in this cold region. Therefore, enhanced mole fractions of nitrogen oxides are primarily a result of long-range transported pollution from anthropogenic or biomass burning sources in Europe, North America, and Asia or of downward transport from the stratosphere (e.g. Liang et al., 2011). A build-up of O_3 precursors during winter in the Arctic free troposphere may have important implications for the tropospheric O_3 budget in the mid-latitudes during late spring and early summer (Gilman et al., 2010). Modelling studies have postulated that air masses originating from the Arctic region can result in the transport of NO_y and NMHC to the North Atlantic and enhance tropospheric O_3 in this region due to the thermal decomposition of PAN (Honrath et al., 1996; Hamlin and Honrath, 2002).

This study utilizes 2 years of continuous measurements and model results to characterize the seasonally varying magnitude of O_3 and its precursors in the remote high altitude Arctic and the potential impact from transported pollution. Year-round measurements of NO_x, NO_y, PAN, O_3 and NMHC from the high altitude Greenland Environmental Observatory at Summit (GEOSummit) station in Greenland are presented. The paper is structured as follows: in Sect. 2, the techniques to measure NO, NO_2, NO_y (total reactive nitrogen oxides $NO_y = NO + NO_2 + PAN + HNO_3 + HONO + \text{others}$), PAN and NMHC are presented and the FLEXPART Lagrangian particle dispersion model utilized in this study is discussed. Section 3.1 discusses the seasonal cycles of O_3 precursors at the measurements site and the NO_y speciation is investigated. In Sect. 3.2, the interannual variability and source contributions to enhanced O_3 precursors from anthropogenic emissions and biomass burning are discussed. Finally, a summary of the main findings is given in Sect. 4.

ACPD
14, 13817–13867, 2014

2 Experimental methods

2.1 GEOSummit Station

Measurements of NO_x, NO_y PAN and NMHC were performed at the GEOSummit Station (hereafter called Summit), Greenland (72.34° N, 38.29° W, 3212 m.a.s.l) from July 2008 to July 2010. Inlets for the instruments were installed ~ 7.5 m above the snowpack on a meteorological tower located approximately 660 m south-west of the main camp within the "clean air" sector. Tubing and cables were routed through a heated pipe to a buried laboratory facility.

2.2 Measurements

2.2.1 Nitrogen oxides

Measurement of NO, NO_2 and NO_y were performed with an automated O_3 chemiluminescence detection system (Ridley and Grahek, 1990). The system was developed at Michigan Technological University and is based on the same design that was used in Newfoundland in 1996 (Peterson and Honrath, 1999) and subsequently installed at the Pico Mountain Site from 2002 to 2010 (Val Martín et al., 2006). NO_2 and NO_y were detected by chemiluminescence after reduction to NO using a photolytic NO_2 converter (Kley and Mcfarland, 1980) and a gold-catalyzed NO_y converter in the presence of CO, respectively (Bollinger et al., 1983; Fahey et al., 1985). NO_y is given as the sum of reactive nitrogen oxides. In the Arctic, NO_y is primarily comprised of NO, NO_2, PAN, HNO_3, HONO and particulate nitrate (p-NO_3^-). For the instrument used in this study, a photolytic blue LED NO_2 converter (Air-Quality Design Inc., Colorado) was installed. Photolytic converters have lower conversion efficiencies than molybdenum converters, however interferences from other species photolyzing to NO, such as HONO and PAN are reduced (Pollack et al., 2011; Villena et al., 2012). The sample mass flow controllers

ACPD
14, 13817–13867, 2014

(MFC) and the NO_2 and NO_y converters were housed inside the inlet box on the tower to minimize the residence time of NO_y species inside the PFA tubing.

During each measurement cycle of 10 min, the NO and NO_2 signals were recorded as 30 s averages and NO_y signals as 20 s averages, after a period of equilibration in each mode. Zero measurements of NO were performed at the start and end of each measurement cycle by mixing O_3 with the sample upstream of the reaction chamber. The zero signals were measured to determine the interference signal in the reaction chamber, which was then subtracted from the measured signals. Calibration cycles, to determine the sensitivity of the instrument to NO and NO_2 converter efficiency, were performed every 12 h through the standard addition (10 cm^3 min^{-1}) of ~ 1 mmol mol^{-1} of NO in nitrogen (N_2) (Scott Marrin, Scott Specialty Gases) to the sample flow of 650 cm^3 min^{-1} at the inlet on the tower. In addition to the standard calibrations, a calibration was performed every 3 days to determine the conversion efficiency of the NO_y converter and artifacts for NO_y, NO and NO_2 were measured via sampling NO_x free air (Breathing air grade, Airgas, Radnor, PA, USA). The final datasets were corrected for this artifact.

The variability in the 20 and 30 s averaged data was compared to the expected value from photon counting statistics which are treated as a Poisson distribution. Measurements with variability greater than 3 times the Poisson value were then removed from the final dataset (~ 4 % were removed with this filter). Evaluation of these periods shows that they typically occur when the wind direction was from the main camp, confirming that local pollution is the main source of the variability. Additional filtering processes were implemented to remove bad data caused by (1) spikes from electronic noise or intermittent instrument malfunctions; (2) high variability due to periods when the skiway was groomed or periods not captured in the Poisson statistics filter and (3) large negative mole fractions, due to short term fluctuations during the measurement cycle. After the application of all the filtering procedures described above, 90–91 % of the NO, NO_2 and NO_y measurements were included in the final dataset.

The NO, NO_2, NO_x and NO_y data used in this work were further averaged over a 30 min period. NO_x was determined as the sum of the NO and NO_2 measurements during each 10 min cycle. The overall uncertainty for the 30 min data is calculated from the root sum of the squares of the measurement accuracy, artifact uncertainty and precision. Maximum uncertainties for NO, NO_2, NO_x at 50 pmol mol^{-1} are 10 %, 17 % and 19 %. For NO_y, the uncertainty at 200 pmol mol^{-1} is < 20 % and typically 9 %.

Detection limits for the 30 min averages were determined from the 2σ precision of the instrument and error in the artifact. Detection limits for NO, NO_2, NO_x and NO_y are 4 pmol mol^{-1}, 8 pmol mol^{-1}, 9 pmol mol^{-1} and 7 pmol mol^{-1}, respectively. Measurements below the detection limit were included in all averaging calculations to ensure the final values were not biased. Further details on the calibrations performed and the precision and accuracy of the measurements are given in the Supplement.

2.2.2 Peroxy-acetyl nitrate

A commercial PAN gas chromatography analyzer (PAN-GC, Metcon, Inc., Boulder, CO) was installed alongside the NO_{xy} instrument to determine PAN mole fractions. The PAN instrument is based on gas chromatography with electron capture detection (GC-ECD). The instrument was equipped with a preconcentration unit to improve the detection limit whilst allowing for PAN sampling every 10 min. The preconcentration unit traps PAN and carbon tetrachloride (CCl_4) on a peltier cooled (5 °C) capillary column prior to injection onto the main GC column which was set to a temperture of 13 °C to reduce the thermal decomposition of PAN. Ultra-pure nitrogen gas (99.9999 % purity) was used as the carrier gas for the PAN-GC.

The instrument was calibrated approximately every week using a known amount of PAN, which was photochemically produced from the same NO-calibration gas used for the NO_{xy} instrument described in Sect. 2.2.1. The NO gas was delivered to a reaction cell inside the PAN calibration unit which contained a UV mercury lamp to photolyze an excess of acetone (in zero air) which reacts with the NO gas to form PAN. The PAN

ACPD
14, 13817–13867, 2014

calibration gas was sent to the inlet on the tower and then sampled by the GC-ECD. The conversion efficiency of NO to PAN was determined at the beginning and end of the measurement period through the standard addition of NO/NO_2 to the NO_{xy} instrument. The conversion efficiency remained relatively constant throughout the measurement period at 96 ± 1 %.

The sensitivities determined from the weekly PAN calibrations were interpolated to the measurements to take into account any drifting. CCl_4 was also used as an internal reference during periods when calibrations were not taken (Karbiwnyk et al., 2003). The atmospheric concentration of CCl_4 should be relatively constant; therefore any changes in the CCl_4 peak area would be caused by changes in the instrument sensitivity. During a period between 28 February 2009 and 17 May 2009 there was a gap in the calibrations caused by a blockage in the tubing that delivered the PAN calibration gas to the inlet. During this period the relationship between the CCl_4 peak area and PAN sensitivity from the previous calibrations was used to obtain the PAN sensitivity. Over the duration of the measurement period the detector became dirty resulting in drifting and a noisy baseline. Due to this issue no data after 28 April 2010 were included in the analyses here.

Similarly to the NO_x and NO_y data, the PAN measurements were averaged over 30 min. The total uncertainty for the 30 min averaged PAN mole fractions was determined from the precision of the instrument (estimated as $2\sigma N^{0.5}$, where N is the number of points averaged in 30 min ($N = 3$)) and the uncertainty in the calibration standard. Uncertainty in the PAN calibration standard is associated with uncertainties in (a) the calculation of the NO addition, (b) the conversion of NO to PAN from the calibration unit and (c) variability in the PAN sensitivity between calibrations. The total uncertainty was estimated to be 16 % during normal operation. This value increased to 22 % during the period in spring 2009 when there were no calibrations.

The limit of detection (LOD) of the instrument was estimated from the peak to baseline noise ratio. The LOD is defined as the mole fraction giving a signal to noise (S/N) ratio of 3. The baseline noise was determined from a region just after the PAN peak for

ACPD
14, 13817–13867, 2014

each chromatogram. The limit of detection was highest during the first few months of operation up to November 2008 with a median value of 41 $pmol\,mol^{-1}$. Despite the high LOD, 88 % of chromatograms were above the LOD during 2008. The LOD improved after this period with a median value of 15 $pmol\,mol^{-1}$. The final PAN data set was not filtered for wind direction as analyses showed that there was no obvious influence from camp pollution on the PAN measurements.

2.2.3 Non-methane hydrocarbons

NMHC were continuously sampled using a fully automated and remotely controlled GC system that was specifically designed for this study. Details of the setup at Summit are given in Helmig et al. (2014a). The GC is a further development of the instrument operated at the Pico Mountain Observatory and described in detail by (Tanner et al., 2006). The instrument provided ~ 6000 ambient measurements of C_2–C_6 hydrocarbons, in addition to ~ 1000 blank and standard runs from June 2008 to July 2010. The inlet for the GC instrument was installed on the same tower as the PAN, NO_y and NO_x inlets. The instrument relies on a cryogen-free sample enrichment and injection system. All consumable gases were prepared at the site with a hydrogen generator, compressor, and air purification system. Aliquots of the sample stream were first passed through a water trap to dry the air to a dew point of −30 °C, then through an ozone scrubber, and NMHC were then concentrated on a Peltier-cooled (−25 °C) multi-stage adsorbent trap. Analysis was accomplished by thermal desorption and injection onto an aluminum oxide (Al_2O_3) porous layer open tubular (PLOT) column for cryogen-free separation on a SRI Model 8610 GC with flame ionization detection (FID). Blanks and standard samples were injected regularly from the manifold. The gravimetric and whole air standards that were used were cross-referenced against our laboratory scale for volatile organic compounds, which has been cross-referenced against national and international scales, including through two previous audits by the World Calibration Centre for VOC. At 100 pptv mole fraction, analytical accuracy and precision are typically better than

3–5 %, yielding a combined uncertainty estimate of ∼ 5 %. The instrument achieves low single digit pmol mol^{-1} detection limits.

2.2.4 Ozone

Surface O_3 was measured by an O_3 analyzer located in the Temporary Atmospheric Weather Observatory (TAWO) building a few hundred meters from camp by the National Oceanic and Atmospheric Administration (NOAA) as part of the core atmospheric measurements that began in 2000 (Petropavlovskikh and Oltmans, 2012). Hourly averaged data for 2008, 2009 and 2010 were downloaded from the Earth System Research Laboratory Global Monitoring Division (ESRL-GMD) website (http://www.esrl.noaa.gov/gmd/dv/data/).

2.2.5 FLEXPART

The Lagrangian particle dispersion model FLEXPART was utilized to identify potential periods when polluted air masses impacted the measurement site. FLEXPART simulates atmospheric transport using wind fields from global forecast models to determine source to receptor pathways of air masses (Stohl et al., 2005). The model was driven with meteorological analysis data from the European Centre for Medium Range Weather Forecasts (ECMWF) and run backward in time in so-called "retroplume" mode (Stohl et al., 2003). Every 3 h 40 000 particles were released from the measurement site location and followed backwards in time for 20 days. Sensitivities to anthropogenic and fire emissions were determined during the backwards simulations and are proportional to the particle residence time over the source areas. In this work a black carbon tracer was used to simulate both anthropogenic (BC_{anthro}) and biomass burning emissions (BC_{fire}). The BC tracer was susceptible to both wet and dry deposition during transport. The wet deposition process is simplified in the simulations (no ageing of BC with conversion from hydrophobic to hydrophilic properties) and may result in an

ACPD
14, 13817–13867, 2014

underestimation of the BC tracer (Stohl et al., 2013). However, for this study the tracer was only used to identify events; therefore absolute BC values were not required.

3 Results and discussion

3.1 Seasonal cycles

3.1.1 Reactive nitrogen oxides

Figure 1a–d shows the statistical analyses of the monthly averaged NO_x, NO_y, and PAN ambient mole fractions, respectively, during the measurement period from July 2008 to July 2010, and results for O_3 from January 2008 to December 2010. A malfunction with the NO_{xy} instrument resulted in missing NO_x and NO_y data from 24 November 2008 to 30 March 2009, hence the number of 30 min averages included in the monthly distribution is much lower for December to March than for other months as indicated by the values at the top of each plot. Seasonal cycles are observed in measured ambient mole fractions of NO_x, NO_y and PAN, with higher levels for all species during the late winter/early spring period and lower mole fractions from summer to fall. The positively skewed whiskers indicate that air masses with elevated levels of the measured species were sampled year round. Anthropogenic and biomass burning emissions transported to the site from North America and Europe are a major source of these enhancements in NO_x, NO_y and PAN (see Sect. 3.2). Observations from the Arctic Research of the Composition of the Troposphere from Aircraft and Satellites (ARCTAS) mission in 2008 show that the transport of air from the Arctic stratosphere to the upper troposphere may also result in elevated levels of O_3 precursors such as NO_x, HNO_3 and PAN above 5 km (Liang et al., 2011). Therefore, high mole fractions observed in PAN, NO_y and NO_x, may also be the result of sampling air masses mixed with those originating from the stratosphere and upper troposphere.

ACPD
14, 13817–13867, 2014

Table 1 gives a statistical summary for the monthly averages of PAN, NO_y, NO_x and O_3 during 2008–2010. Maxima in monthly mean mole fractions of PAN and NO_y were observed in April with mean levels of 241 ± 77 (1σ) pmol mol^{-1} and 321 ± 98 pmol mol^{-1} respectively. PAN mole fractions at Summit and the magnitude of the PAN springtime peak are consistent with observations at other high latitude sites such as Zeppelin Mountain, Svalbard (Beine et al., 1997; Solberg et al., 1997; Beine and Krognes, 2000) and Alert, Northwest Territories, Canada (Worthy et al., 1994; Dassau et al., 2004). There is a rapid transition towards lower levels of PAN in the summer, with a minimum mean monthly average of 66 ± 29 pmol mol^{-1} in July. NO_y mole fractions do not decrease as quickly from spring to summer as PAN and reach a minimum monthly average of 100 pmol mol^{-1} in September. We find that the PAN and NO_y summer mole fractions observed here are comparable to previous measurements performed at the same site in 1998 and 1999, when observed PAN levels were typically 20–150 pmol mol^{-1} and NO_y levels ranged between 100–300 pmol mol^{-1} (Honrath et al., 1999; Ford et al., 2002). The slower decrease in NO_y from spring to summer, compared to PAN, is a result of the presence of NO_x and odd NO_y (odd $NO_y = NO_y - PAN - NO_x$) over the summer months and is discussed further below.

The seasonal cycle of PAN is governed by the rate of thermal decomposition and transport patterns. The warmer summer temperatures result in the decomposition of PAN during long range transport, additionally, during the summer months the polar front recedes north, thus reducing the potential for anthropogenic emissions to reach the measurement site (Beine and Krognes, 2000; Stohl, 2006). Measurements have shown that PAN is typically the largest contributor to NO_y in the Arctic, due to the rapid formation of PAN near the source region and a long lifetime in the free troposphere (Solberg et al., 1997; Munger et al., 1999; Ford et al., 2002; Alvarado et al., 2010; Singh et al., 2010; Liang et al., 2011). However, there have been very few studies on the seasonal variability of the NO_y speciation in the Arctic due to limited measurements over winter months. The full annual cycle of NO_y contributions from PAN and NO_x during this study provides some information on the NO_y speciation, year round at Summit.

The results plotted in Fig. 2 show that PAN is the dominant form of NO_y all year round, with monthly average [PAN]/[NO_y] ratios reaching a maximum of 78 % in April and a minimum of 49 % in July. Over the summer, NO_x contributes approximately 10–13 % to the total NO_y. In winter this decreases to $\lesssim$ 4 % and often NO_x levels were below the dectection limit of the instrument. What is particularly striking about the NO_y speciation shown in Fig. 2 is that odd NO_y levels can be significant, particularly over winter, when they reach a maximum monthly mean of 95 ± 36 pmol mol^{-1} (mean ± SD) in February. Odd NO_y decreases to approximately 30–50 pmol mol^{-1} in the summer months; however, this still accounts for ~ 20–38 % of the total NO_y during this period.

Snowfall rates increase during the summer months over Summit (Dibb and Fahnestock, 2004) therefore an increase in deposition of water-soluble species such as HNO_3 to the snowpack may result in the depletion of ambient odd NO_y in the summer. The increase in solar radiation may also play an important role in the reduction of odd NO_y species in the summer. Solberg et al. (1997) observed a decrease in odd NO_y with increasing solar UV radiation in Spitsbergen, Norway. The authors suggested that species such as HONO, HNO_3, NO_3, N_2O_5, HO_2NO_2, and alkyl nitrates may contribute to NO_y over the winter with the impact reducing in spring due to an increase in photolysis. A study on the seasonal variability of alkyl nitrates at Summit in 1998–1999 found that the light C_1–C_4 alkyl nitrates peak through late winter until April with total mole fractions between 30 and 42 pmol mol^{-1} (Swanson et al., 2003). Therefore, alkyl nitrates could account for a large portion of the odd NO_y observed during the winter months at Summit. However, there still remains a large fraction of NO_y unaccounted for over winter and further measurements are required to determine both the species and sources of this odd NO_y.

The seasonal cycle for NO_x does not follow PAN and NO_y at Summit. As shown in Table 1, monthly mean NO_x levels peak one month later than NO_y and PAN, increasing from 6 ± 11 pmol mol^{-1} in February to 29 ± 24 pmol mol^{-1} in May, coinciding with an increase in solar radiation. Thus, the relative contribution of NO_x to NO_y maximizes over the summer when NO_x is still high but PAN levels decrease. The thermal decomposition of PAN is a possible source of NO_x during spring and summer months, however, the contribution is expected to be very small in this high latitude region as temperatures during the measurement period were always below 0 °C (Beine et al., 1997). Thus, the increase of NO_x with radiation in spring suggests a possible photochemical source. The role of snowpack emissions on NO_y species within the arctic boundary layer is still uncertain, however, studies have suggested that photochemical reactions within the snowpack may result in the release of NO_x and HONO to the overlying atmosphere (e.g., Honrath et al., 1999, 2000a, b, 2002; Munger et al., 1999; Beine et al., 2002; Dibb et al., 2002; Dominé and Shepson, 2002; Beine et al., 2003; Grannas et al., 2007).

During late spring to summer, odd NO_y species can contribute over twice as much as NO_x to the total NO_y. To investigate the source of these species and the possible impact from snowpack photochemistry we have analyzed the diurnal variability of NO_x, NO_y and odd NO_y at Summit. Our measurements of NO_x and NO_y mole fractions at a height of ~ 7.5 m above the snowpack display clear diurnal cycles from April–June (Fig. 3a, b). It is observed that the amplitude of the NO_y diurnal cycle is greater than for NO_x, with average diurnal amplitudes of 33 pmol mol^{-1} and 14 pmol mol^{-1} for NO_y and NO_x respectively. It has been hypothesized that photochemically produced odd NO_y species such as HNO_3 and HONO may account for some of the NO_y diurnal variability at Summit (Ford et al., 2002). An analysis of the diurnal cycle for odd NO_y (Fig. 3c) averaged over April–June from 2008–2010 shows that the odd NO_y peaks just after solar noon in our measurements, suggesting a photochemically produced odd NO_y species may be present. The diurnal variability of ambient NO_y species above the snowpack is further complicated by vertical mixing and boundary layer dynamics, which may vary with season. For example, the downward transportation of pollution from aloft due to a growing boundary layer may result in a daytime maximum in NO_x and NO_y, which then decreases at night due to surface uptake. There is also a possible contribution to odd NO_y in the summer from long range transport of reactive nitrogen species such as HNO_3 and alkyl nitrates as these species have previously been observed in anthropogenic and biomass burning plumes in the Arctic (Liang et al., 2011; Wespes

ACPD
14, 13817–13867, 2014

et al., 2012). It should also be noted that some of the variability in the NO_y speciation discussed here may be influenced by uncertainties in the PAN measurements which increased in spring 2009. The year-round measurements obtained from Summit in 2008–2010 provide new insight on the relative role of photochemistry and boundary layer stability on diurnal cycles of nitrogen oxides and is the subject of future investigation.

3.1.2 Non-methane hydrocarbons

Figure 4 shows the results for the C_2–C_5 alkane NMHC measured during 2008–2010 at Summit. The NMHC show a strong seasonal cycle with maximum mole fractions during the winter and early spring period and a rapid decline towards the summer due to an increase in photochemical processing. The monthly mean averages for the C_2–C_5 NMHCs are given in Table 2. The phase of each NMHC is shifted due to the rate of reaction with OH. The lightest of the NMHC shown in Fig. 4 is ethane (C_2H_6), which peaks in March with a monthly mean of 1974 ± 209 pmol mol^{-1} (mean ±1σ) and reaches a minimum of 633 ± 65 pmol mol^{-1} in August. Heavier NMHC have lower mole fractions and peak earlier in the year and reach a minimum earlier in summer as their rate of reaction with OH is much faster. The seasonal cycle of NMHC at Summit including NMHC firn air measurements from 2008 to 2010 have previously been presented in detail (Swanson et al., 2003; Helmig et al., 2014a, b).

The seasonality of NMHC can provide some insight into the potential for the photochemical production of O_3 in the Artic troposphere. The accumulation of O_3 precursors, such as nitrogen oxides and NMHC over winter has been suggested as a potential in situ source of O_3 that may contribute to the tropospheric O_3 peak observed in spring in the Arctic (e.g., Penkett et al., 1993; Honrath et al., 1996; Monks, 2000; Blake et al., 2003; Wang et al., 2003). Measurements of NMHC and O_3 during the Tropospheric Ozone Production about the Spring Equinox (TOPSE) campaign show that within the mid-troposphere, total NMHC decreased by ~ 6.2 ppbC from February to May and that O_3 increased by ~ 16 ppbv during the same period (Blake et al., 2003). The data from

ACPD
14, 13817–13867, 2014

this study show similar results for NMHC, with the sum of the C_2–C_6 NMHC decreasing by ~ 4.4 ppbC from February to May. The magnitude of the O_3 increase, at ~ 8 ppbv, is smaller than observed during TOPSE, however, the photochemical processing of NMHC in spring may contribute to the spring time peak of O_3 over Greenland.

3.2 Variability in ozone and its precursors from anthropogenic and biomass burning emissions

In this section the interannual and short term variability in the measured species at Summit from 2008–2010 due to variability in transport pathways and the relative source contributions of pollutants from North America, Europe and Asia are investigated. Anthropogenic and biomass burning emissions are considered separately, over different seasons.

3.2.1 Winter/spring anthropogenic impacts

Figure 4 shows that there is considerable variability in the NMHC mole fractions superimposed on the seasonal cycle; in particular during the winter months, suggesting polluted air masses were transported to the measurement site during this period. Mean $\pm 1\sigma$ mole fractions of ethane were $1.86 \pm 0.24\,\mathrm{nmol\,mol^{-1}}$ in December 2008 to March 2009 and $1.69 \pm 0.31\,\mathrm{nmol\,mol^{-1}}$ for December 2009 to March 2010. The 95th percentile values were the same for the two periods ($2.2\,\mathrm{nmol\,mol^{-1}}$) suggesting that polluted air masses had a strong impact during both seasons. However, the average background level (given by the 20th percentile of the measurements during each period) was lower in 2009/2010 ($1.4\,\mathrm{nmol\,mol^{-1}}$) than 2008/2009 ($1.6\,\mathrm{nmol\,mol^{-1}}$) suggesting that in 2009/2010 there was a greater number of clean air masses or periods with low emissions impacting the site.

FLEXPART tracer simulations indicate that during the months December to March, biomass burning events were limited to a ~ 1 week period in March 2009 (see Table 3); therefore, we focus the analysis on anthropogenic emissions between these months.

Discussion Paper | Discussion Paper | Discussion Paper | Discussion Paper |

ACPD

14, 13817–13867, 2014

Seasonal variability of nitrogen oxides and NMHC at Summit

L. J. Kramer

To investigate the source of the observed variability and the impact on ozone precursor levels at Summit, the anthropogenic tracer from FLEXPART retroplume simulations (BC_{anthro}) and NMHC emissions ratios were used to determine changes in the transport pathways and relative source contributions of anthropogenic emissions from different continents.

An event with pollution transport was defined as identified when the BC_{anthro} tracer was greater than 75th percentile of the total BC_{anthro} during the 2 year measurement period (corresponding to $BC_{anthro} > 0.0082\,\mathrm{pmol\,mol^{-1}}$) for a minimum of 12 h. The FLEXPART temporal resolution for backward simulations is 3 h, so identifying events when the BC_{anthro} was enhanced for at least 12 h ensured that significant polluted air masses impacted the site and also allowed for some temporal mismatches in simulated and observed plume arrivals. Using these thresholds, 42 events were identified in total for the periods December to March 2008/2009 and December to March 2009/2010 (21 events each season). FLEXPART retroplume analysis also provides information on the source contribution to these events, shown in Figs. 5 and 6. In 2008/2009, the BC_{anthro} tracers originating from North America and Europe accounted for 26 % and 69 %, respectively, to the total BC_{anthro} tracer mass during the pollution events. In 2009/2010, North American emissions were much lower, contributing only 13 % of the total BC_{anthro} tracer mass, with European emissions dominating with 82 %. In both years impacts from Asian emissions were low (< 6 %) and negligible from other continents. The mean weighted age of the plume was calculated for each FLEXPART retroplume, to determine the typical transport time for the events. The median time for polluted air masses to be transported to the site was approximately 11 days.

During each event, the mean ΔPAN, ΔNO_y, ΔNO_x,ΔO_3 and ΔC_2H_6 were determined, where Δ is the enhancement above background levels (determined as the 20th percentile for each species each month). For the 42 anthropogenic events identified, the mean enhancements during each event ranged between −35 and +273 $\mathrm{pmol\,mol^{-1}}$ for PAN, 0 to +25 $\mathrm{pmol\,mol^{-1}}$ for NO_x, −17 to +336 $\mathrm{pmol\,mol^{-1}}$ for NO_y, −3.9 to 7.5 for O_3, and −0.3 to +1.0 $\mathrm{nmol\,mol^{-1}}$ for C_2H_6, with negative results representing less than

ACPD
14, 13817–13867, 2014

20 % of the events for PAN, ethane, NO_x and NO_y and 26 % for O_3. Negative enhancement values may be associated with erroneous transport simulated by FLEXPART as the mean enhancement for each species is dependent on the timing and length of the events as determined from FLEXPART. During the winter/spring period, there is a large gradient in O_3 precursors with latitude (e.g. Moxim et al., 1996; Blake et al., 2003), therfore, the transport of air masses from the south may also result in lower total mole fractions at Summit, despite pollution input from emission sources.

Figures 7 and 8 show a time series of the measurements between December and March for 2009/2010 and 2008/2009, respectively. During these periods, events with elevated ethane, NO_y, PAN and NO_x levels are observed; however, what is particularly interesting is that during some of these events, low O_3 mole fractions ($\Delta O_3 < 0$) were measured. Analyses of ΔO_3 and FLEXPART BC tracer masses from July 2008 to July 2010 show that decreases in O_3 below the background level (when ΔO_3 was negative for at least 12 h and reached a minimum ΔO_3 level below $-2\,\mathrm{nmol\,mol^{-1}}$) were observed throughout the year. During April to September 45 events with low ozone were observed, however, these events were typically associated with low levels of pollution with only 10 out of the 45 events classified as polluted (as indicated by either high FLEXPART BC_{anthro} (> 75th percentile) or BC_{fire} (> 90th percentile) tracers). For the remaining 35 events enhancements in NO_y, PAN and ethane were either low or negative, suggesting pollution levels were minimal in the sampled air masses.

Decreases in O_3 (where the minimum $\Delta O_3 < -2\,\mathrm{nmol\,mol^{-1}}$) that coincided with anthropogenic pollution events were observed during 28 periods from July 2008 to July 2010, with 21 of these events occurring between October and March, when sunlight is at a minimum. Thus, it is possible that the decrease in O_3 observed during winter/early spring is due to titration of O_3 by NO within the sampled air mass soon after emission (Eneroth et al., 2007; Hirdman et al., 2010). For example, from 23 to 31 January 2010 (indicated by the shaded area in Fig. 7), O_3 decreased rapidly during two periods, coinciding with increases in O_3 precursors. Using the vertically integrated emission sensitivity (also called the total column sensitivity, measured in nanosecond

ACPD
14, 13817–13867, 2014

meters per kg) simulated by FLEXPART, the overall pathways of the air masses during these events can be determined. As shown in Fig. 9a, the air mass on 23 January originated from Northern Europe and was transported to Summit in only a few days. The mean weighted age of the plumes estimated from FLEXPART during this period decreased from ~ 15 to 8 days (Fig. 7).

Studies have shown that NMHC ratios can provide an indication of the photochemical aging of the air mass as the rate of reaction of different NMHC, and hence the ratio, is dependent on the amount of photochemical processing that occurs during transport (Parrish et al., 2004; Helmig et al., 2008; Honrath et al., 2008). High photochemical processing results in a decrease in the ln([propane]/[ethane]) ratio as propane reacts more readily with OH than ethane. The two low ozone events between 23 and 31 January 2010, coincided with enhancements in the ln([propane]/[ethane]) ratio suggesting low photochemical processing, and the impact of fresher air masses at the site. However, care must be taken when interpreting this result as dilution of the measured species during transport will also have an impact on the mole fractions measured at the site. PAN and ethane reached peaks of 188 pmol mol^{-1} and 3 nmol mol^{-1}, respectively, during the event on 23 January, supporting the FLEXPART analyses which indicated a polluted air mass originating from Europe was sampled at the site (note there were no NO_y or NO_x data available during this period). Ozone, however, decreased by 6.2 nmol mol^{-1} below the monthly background level ($O_{3(\text{bkg})}$ = 41.6 nmol mol^{-1}) to reach a minimum level of 35.4 nmol mol^{-1}. The FLEXPART retroplume on this day shows that air mass resided in the lower ~ 2 km during transport, until 1 day upwind when the air mass ascended over the surface of Greenland to the measurement site (Fig. 9a), thereby reducing the potential to mix with high O_3 from stratospheric origin. In contrast, a few hours later the transport patterns quickly changed, and the air masses sampled at Summit originated from high altitudes over North Canada, as shown in Fig. 9b. As a result, O_3 levels increased and PAN and ethane decreased back toward their background levels ($\text{PAN}_{(\text{bkg})}$ = 72 pmol mol^{-1}, $C_2H_{6(\text{bkg})}$ = 1.55 nmol mol^{-1}). Air originating from the high Arctic region was sampled at the site until 29 January, when the retroplume moved southward and air masses residing in the lower troposphere over North America transported polluted air to Summit (Fig. 9c). From 29–30 January, ethane, NO_y, PAN and NO_x all increased again by 1.3 nmol mol^{-1}, 267 pmol mol^{-1}, 146 pmol mol^{-1} and 32 pmol mol^{-1} respectively, from the calculated monthly background levels, and O_3 decreased by 2 nmol mol^{-1}.

Analyses of all the pollution events over winter and early spring indicate that low O_3 events from December to March typically coincide when sampling air masses originating from either Europe or North America, which have resided in the lower troposphere until ascending over Greenland to the measurement site (examples of FLEXPART retroplumes are shown in Fig. S1a–e in the Supplement). In contrast, periods identifed during winter as pollution events with positive O_3 enhancement values occurred when the air masses resided in the mid-troposphere during transport to the site (Fig. S2a and b in the Supplement), thus allowing for greater mixing with air from high tropospheric or stratospheric origin.

In this study the impact from anthropogenic emissions, as identified through FLEXPART retroplume analyses, were the primary focus. However, enhancements in the measured species were also observed during periods which are not correlated with pollution events simulated by FLEXPART. For example, between 12 February and 1 March 2010, Fig. 7 shows two periods when enhancements in PAN, NO_y, and ethane that do not coincide with high FLEXPART BC_{anthro} tracer are observed. Analysis of the BC_{fire} tracer from FLEXPART also indicated no pollution plume from biomass burning origin. The retroplume analysis shows that air masses from these two events were transported over the far north region of Canada and remained in the arctic for many days before arriving at Summit. It is unlikely that the air sampled was from a stratospheric origin, as ethane levels were high and ozone decreased during these events. It is possible that there may be an error in the simulated retroplume by FLEXPART or that the pollution originated prior to the 20 day simulation. Further investigations are necessary to determine the cause of these events and enhancements in the O_3 precursors.

ACPD
14, 13817–13867, 2014

3.2.2 Summer impact from biomass burning and anthropogenic events

The extended whiskers shown on the plots in Fig. 1 indicate a large amount of variability in the O_3 precursors during the summer months. Radiation, surface emissions, boundary layer height and changes in air mass sampling may all contribute to the variability observed, which is typically in the range of hours to days. Anthropogenic emission impacts tend to be lower in the summer due to reduced transport from source regions, however pollution from anthropogenic and, especially, BB emissions can still impact the center of Greenland (Stohl, 2006), resulting in elevated mole fractions for short periods (Stohl et al., 2006). Studies based on aircraft measurements and models during the ARCTAS campaigns in both spring and summer 2008 show that biomass and anthropogenic plumes can result in elevated NO_x, NO_y, PAN and hydrocarbons in the Arctic (e.g., Alvarado et al., 2010; Singh et al., 2010; Hornbrook et al., 2011; Liang et al., 2011).

The BC_{fire} tracer from FLEXPART was used to identify periods at Summit that were potentially impacted by BB emissions. FLEXPART has been used to identify long range transport of biomass burning emissions in many studies (e.g., Brioude et al., 2007; Stohl et al., 2007; Lapina et al., 2008; Quennehen et al., 2011, 2012; Schmale et al., 2011; Cristofanelli et al., 2013). However, due to potential inaccuracies with the FLEXPART simulation of transport pathways, fire identification and tracer emission uncertainties, BB events identified may be under or overestimated. Biomass burning events were characterized as having a FLEXPART BC_{fire} tracer > 90th percentile ($\simeq 7\,\mathrm{pmol\,mol^{-1}}$). In total, 13 events were observed between July 2008 and July 2010 ranging in duration between 12 and 252 h. Details regarding the start date, duration, mean plume age, FLEXPART tracer levels and trace gas levels for each event are shown in Table 3. A more conservative threshold was applied here than for the anthropogenic emissions in Sect. 3.2.1, so the events identified had significant BB but small anthropogenic signatures. Of these 13 events, 2 were identified as having potentially high anthropogenic signatures (BC_{anthro} > 75th percentile) and were most likely plumes

ACPD
14, 13817–13867, 2014

of mixed anthropogenic and biomass burning emissions, 5 events were identified as having medium anthropogenic signatures (75th percentile > BC_{anthro} > 50th percentile) and the remaining 6 events were classified as having low anthropogenic signatures.

The analysis of the source contribution from FLEXPART shows that the majority of the BB events (9 out of 13) originated in North America, with BB events originating in Europe all occurring in March 2009. To ensure that the results were not biased through only identifying events during the measurement period, a statistical analysis of all the FLEXPART data from 2008, 2009 and 2010 was performed. For these 3 years, 23 BB events lasting longer than 12 h (both with and without anthropogenic mixing) were identified. Of these 23 events, ~ 67 % of the BC_{fire} tracer originated from North America, 15 % from Europe and 19 % from Asia, confirming that North America is the primary source of BB emissions impacting Summit.

Analyses of O_3 and its precursors at Summit show that the mean enhancements for PAN, NO_x, NO_y and C_2H_6 during the BB events identified by FLEXPART are highly variable (Table 3). Values ranged between −4.4 and 12.4 nmol mol^{-1} for ΔO_3, −7.9 to 90.4 pmol mol^{-1}for ΔPAN, 0.6 to 24.5 pmol mol^{-1}for ΔNO_x, −5.6 to 141.1 pmol mol^{-1} for ΔNO_y and −22.9 to 338.0 pmol mol^{-1} for ΔC_2H_6, for the 11 BB events characterized as having low/medium anthropogenic signatures. When considering only those events with low anthropogenic signatures, the results show that air masses sampled with potential BB contributions have ΔO_3 ranging between −4.4 and 10.8 nmol mol^{-1}, with positive enhancements during 4 out of 5 events. These enhancements are comparable to those by Thomas et al. (2013) who estimated ozone production of up to 3 nmol mol^{-1} in aged BB plumes in the mid to upper-troposphere (peaking at 7 km) over Greenland. Our results suggest that in the lower troposphere the enhancement may even be greater. However, the enhancement values presented here can only be considered as best estimates based on the FLEXPART transport model simulations. Additionally, the long transport times from source region to the measurement site suggest significantly aged BB plumes, with mean weighted plume ages for the events ranging between 9–18 days (median 14 days). These aged plumes will be well mixed

ACPD
14, 13817–13867, 2014

Seasonal variability of nitrogen oxides and NMHC at Summit

L. J. Kramer

with the background air, therefore, separating the pollution impacts from background levels is challenging. For example, in 2008 FLEXPART indicated that a BB event impacted the measurement site from 25–26 July (event 1). The total column sensitivity from the FLEXPART retroplume (see Fig. 10) shows that the air masses arriving at the site during this event in July originated from a region with BB sources over Canada and Alaska and was transported in the lower troposphere over the Arctic Ocean. The air resided over the Arctic Ocean for ~ 4 days before ascending to Summit; therefore, it is likely that the polluted air containing BB emissions mixed with cleaner air from this region. As a result, measurements during this event show small positive enhancements for NO_x and C_2H_6, and negative values for ΔO_3, ΔPAN and ΔNO_y.

The largest BB event identified by FLEXPART was observed in August 2008, when the BC_{fire} tracer indicated BB plumes impacted the site continuously from 3 August to 14 August, peaking at ~ 91 $pmol\,mol^{-1}$, as a result of large wildfires in Canada. We find O_3 and its precursors were all positive during this period, with mean enhancements of 56.5, 19.4 and 141.1 $pmol\,mol^{-1}$ for ΔPAN, ΔNO_x and ΔNO_y respectively, and 10.5 $nmol\,mol^{-1}$ for ΔO_3. A closer analysis of the measurements in Fig. 11 shows that O_3 was consistently high during the event. Analysis of the FLEXPART total column sensitivity indicates that during this event air masses were often transported at high altitudes in the free troposphere, enhancing the probability of mixing with high ozone from stratospheric origin, which may contribute to the elevated O_3 levels that were observed (Alvarado et al., 2010; Roiger et al., 2011).

Anthropogenic events during the summer months (April–September) were identified using the same threshold for winter/spring as in Sect. 3.2.1. During the measurement period, 28 events were identified with mean enhancement values up to 16 $nmol\,mol^{-1}$, 28 $pmol\,mol^{-1}$, 237 $pmol\,mol^{-1}$, 205 $pmol\,mol^{-1}$, and 1.0 $nmol\,mol^{-1}$ for ΔO_3, ΔPAN, ΔNO_x, ΔNO_y and ΔC_2H_6, respectively. The air masses of anthropogenic origin primary originated from Europe with a mean plume age ranging between 7 to 15 days. The maximum enhancements during anthropogenic events are much larger than those from

ACPD
14, 13817–13867, 2014

the BB events, suggesting that air masses containing anthropogenic emissions may have a larger impact on levels of O_3 and precursors at Summit during the summer.

4 Summary

These anlayses of NO_y, NO_x, PAN, NMHC and O_3 from the high altitude GEOSummit Station in Greenland show that PAN is the dominant species of NO_y at the site, year round, ranging from 49 % in the summer months to 78 % in spring. However, the NO_y seasonal cycle does not follow that of PAN, due to significant contributions from NO_x in the summer and odd NO_y species during both summer and winter. We hypothesize that alkyl nitrates may account for a large portion of the odd NO_y observed in winter and that photochemically produced species such as NO_x and HONO within the snowpack may impact the NO_y budget during summer. However, these hypotheses cannot be confirmed without coincident measurements of indivdual NO_y species and alkly nitrates above the snowpack.

Analyses of the C_2–C_6 alkane NMHC data show that there is a large build up of NMHC during the winter period in the atmosphere above Summit which peaks between January and March. The increase in photochemical processing after polar sunrise coincides with a decrease in NMHC levels during subsequent months. Between February and May total C_2–C_6 NMHC decreased by approximately 4.4 ppbC. The decrease in NMHC may contribute partly to the spring time peak in O_3 observed over the same period. Further analyses using a photochemical model, constrained by the measurements, is needed to evaluate the springtime O_3 photochemical production rate at the measurement site and during subsequent transport downwind (Hamlin and Honrath, 2002).

Rapid changes in the origin of sampled air masses, from regions in Europe, North America and the high latitude Arctic, result in a large variability in the measured species. FLEXPART BC tracers and retroplume simulations show that European sources dominated the anthropogenic emissions impacting the site in

ACPD
14, 13817–13867, 2014

December–March contributing to 69 % of the anthropogenic BC tracer in 2009 and 82 % in 2010. In contrast, North America is the primary source of BB polluted air masses impacting the site in the summer. However BB emissions from Asia and Europe impact the site to a lower degree. Individual pollution events during December to March 2008/2009 and 2009/2010 show polluted air masses often result in ozone precursors above the background level with mean enhancements up to 336 $pmol\,mol^{-1}$, 273 $pmol\,mol^{-1}$, 25 $pmol\,mol^{-1}$ and 1.0 $nmol\,mol^{-1}$ for NO_y, PAN, NO_x and ethane respectively.

O_3 levels at Summit are typically higher than those observed at lower elevation Arctic sites due to a stronger influence of transport from the stratosphere and a reduction in ozone depletion events from halogens (Helmig et al., 2007a, b; Hirdman et al., 2010). Short periods with reduced ozone are observed throughout the year. During the summer months, these low ozone events tend to occur when the sampled air masses contain low levels of pollution. In contrast, during the winter, low ozone coincided with the occurrence of polluted air masses that have been transported in the lower troposphere to the site, possibly due to the occurrence of O_3 titration and reduced mixing with high background O_3.

FLEXPART tracer simulations indicated that biomass burning emissions transported to Summit during the summer in 2008–2010 primarily originated from North America. Plumes originating from BB events in Europe were only present during a short period in March 2009. The analyses focused on 11 BB events during the measurement period which did not have large anthropogenic signatures. During these events O_3 and precursor levels were typically enhanced within the BB plumes with ΔO_3 levels up to 12.4 $nmol\,mol^{-1}$ and ΔPAN, ΔNO_y and ΔC_2H_6 levels enhanced by up to 90.4, 141.1 $pmol\,mol^{-1}$ and 338 $pmol\,mol^{-1}$, respectively. However, we cannot say with confidence here whether the enhanced levels observed were directly as a result of biomass burning emissions or whether they occurred as a result of the plumes mixing with background air at high altitudes. In fact, it was found during the summer months that enhancements in all the measured species were greater when sampling air masses from

ACPD
14, 13817–13867, 2014

anthropogenic origin rather than BB plumes. High NO_y levels observed above the background during the events discussed here may have an impact on snow photochemistry and the subsequent release of NO_x, due to the uptake of NO_y species such as HNO_3 and HONO to the snow pack (Grannas et al., 2007, and references therein). Due to the stability of the Arctic free troposphere the region is an effective reservoir for O_3 precursors. Therefore, the high O_3 precursor mole fractions above background levels in the summer may have important implications for NO_x and O_3 in the mid-latitudes during southerly flow of air masses (Hamlin and Honrath, 2002). However, we find there is a need for future studies to constrain the speciation of NO_y above the snowpack, through year-round coincident measurements of NO_x, PAN, NO_y HONO and HNO_3 determine the sources of odd NO_y in the winter and summer.

The Supplement related to this article is available online at doi:10.5194/acpd-14-13817-2014-supplement.

Acknowledgements. The authors acknowledge support for this project from the NASA ROSES program, grant number NNX07AR26G. J. F. Burkhart and A. Stohl were supported by the Norwegian Research Council in the framework of POLARCAT-Norway. The authors would like to acknowledge Mike Dziobak at Michigan Tech for all his valuable work with the instrumentation and Brie Van Dam and Jacques Heuber from The University of Colorado, Boulder who assisted with the measurements. We would like to thank the 109th Air National Guard and the support staff and science technicians from CH2M Hill Polar Field Services for their valuable assistance and the Danish Commission for Scientific Research for providing access to GEOSummit Station.

References

Alvarado, M. J., Logan, J. A., Mao, J., Apel, E., Riemer, D., Blake, D., Cohen, R. C., Min, K.-E., Perring, A. E., Browne, E. C., Wooldridge, P. J., Diskin, G. S., Sachse, G. W., Fuelberg, H., Sessions, W. R., Harrigan, D. L., Huey, G., Liao, J., Case-Hanks, A., Jimenez, J. L., Cubison, M. J., Vay, S. A., Weinheimer, A. J., Knapp, D. J., Montzka, D. D., Flocke, F. M., Pollack, I. B., Wennberg, P. O., Kurten, A., Crounse, J., Clair, J. M. St., Wisthaler, A., Mikoviny, T.,

ACPD
14, 13817–13867, 2014

Seasonal variability of nitrogen oxides and NMHC at Summit

L. J. Kramer

Yantosca, R. M., Carouge, C. C., and Le Sager, P.: Nitrogen oxides and PAN in plumes from boreal fires during ARCTAS-B and their impact on ozone: an integrated analysis of aircraft and satellite observations, Atmos. Chem. Phys., 10, 9739–9760, doi:10.5194/acp-10-9739-2010, 2010. 13830, 13839, 13841

Barrie, L. A. and Bottenheim, J. W.: Sulphur and nitrogen pollution in the arctic atmosphere, in: Pollution of The Arctic Atmosphere, edited by: Sturges, W., Elsevier Press, New York, 155–183, 1991. 13821

Beine, H. J. and Krognes, T.: The seasonal cycle of peroxyacetyl nitrate (PAN) in the European Arctic, Atmos. Environ., 34, 933–940, doi:10.1016/S1352-2310(99)00288-5, 2000. 13821, 13830

Beine, H. J., Jaffe, D. A., and Herring, J. A.: High-latitude springtime photochemistry, Part I: NO_x, PAN and Ozone Relationships, J. Atmos. Chem., 27, 127–153, 1997. 13820, 13821, 13830, 13832

Beine, H. J., Honrath, R. E., Dominè, F., Simpson, W. R., and Fuentes, J. D.: NO_x during background and ozone depletion periods at Alert: Fluxes above the snow surface, J. Geophys.Res., 107, 4584, doi:10.1029/2002JD002082, 2002. 13832

Beine, H. J., Dominè, F., Ianniello, A., Nardino, M., Allegrini, I., Teinilä, K., and Hillamo, R.: Fluxes of nitrates between snow surfaces and the atmosphere in the European high Arctic, Atmos. Chem. Phys., 3, 335–346, doi:10.5194/acp-3-335-2003, 2003. 13832

Blake, N. J., Blake, D. R., Sive, B. C., Katzenstein, A., Meinardi, S., Wingenter, O. W., Atlas, E. L., Flocke, F., Ridley, B. A., and Sherwood Rowland, F.: The seasonal evolution of NMHCs and light alkyl nitrates at middle to high northern latitudes during TOPSE, J. Geophys. Res., 108, 8359, doi:10.1029/2001JD001467, 2003. 13821, 13833, 13836

Bollinger, M. J., Sievers, R. E., Fahey, D. W., and Fehsenfeld, F. C.: Conversion of nitrogen dioxide, nitric acid, and *n*-propyl nitrate to nitroc oxide by gold-catalzed reduction with carbon monoxide, Anal. Chem., 55, 1980–1986, 1983. 13823

Bottenheim, J. W., Sirois, A., Brice, K. A., and Gallant, A. J.: Five years of continuous observations of PAN and ozone, J. Geophys. Res., 99, 5333–5352, 1994. 13821

Brioude, J., Cooper, O. R., Trainer, M., Ryerson, T. B., Holloway, J. S., Baynard, T., Peischl, J., Warneke, C., Neuman, J. A., De Gouw, J., Stohl, A., Eckhardt, S., Frost, G. J., McKeen, S. A., Hsie, E.-Y., Fehsenfeld, F. C., and Nédélec, P.: Mixing between a stratospheric intrusion and a biomass burning plume, Atmos. Chem. Phys., 7, 4229–4235, doi:10.5194/acp-7-4229-2007, 2007. 13839

ACPD
14, 13817–13867, 2014

Seasonal variability of nitrogen oxides and NMHC at Summit

L. J. Kramer

Browell, E. V., Hair, J. W., and Butler, C. F.: Ozone, aerosol, potential vorticity, and trace gas trends observed at high-latitudes over North America from February to May 2000, J. Geophys. Res., 108, 1–16, doi:10.1029/2001JD001390, 2003. 13821

Cristofanelli, P., Fierli, F., Marinoni, A., Calzolari, F., Duchi, R., Burkhart, J., Stohl, A., Maione, M., Arduini, J., and Bonasoni, P.: Influence of biomass burning and anthropogenic emissions on ozone, carbon monoxide and black carbon at the Mt. Cimone GAW-WMO global station (Italy, 2165 m a.s.l.), Atmos. Chem. Phys., 13, 15–30, doi:10.5194/acp-13-15-2013, 2013. 13839

Dassau, T. M., Shepson, P. B., Bottenheim, J. W., and Ford, K. M.: Peroxyacetyl nitrate photochemistry and interactions with the Arctic surface, J. Geophys. Res., 109, D18302, doi:10.1029/2004JD004562, 2004. 13830

Dibb, J. E., and Fahnestock, M.: Snow accumulation, surface height change, and firn densification at Summit, Greenland: Insights from 2 years of in situ observation, J. Geophys. Res., 109, D24113, doi:10.1029/2003JD004300, 2004. 13831

Dibb, J. E., Talbot, R W., Munger, J. W., Jacob, D. J., and Fan, S. M.: Air-snow exchange of HNO_3 and NO_y at Summit, Greenland, J. Geophys. Res., 103, 3475–3486, 1998. 13821

Dibb, J. E., Arsenault, M., Peterson, M. C., and Honrath, R. E.: Fast nitrogen oxide photochemistry in Summit, Greenland snow, Atmos. Environ., 36, 2501–2511, doi:10.1016/S1352-2310(02)00130-9, 2002. 13832

Dominé, F. and Shepson, P. B.: Air-snow interactions and atmospheric chemistry, Science, 297, 1506–1510, doi:10.1126/science.1074610, 2002. 13832

Eneroth, K., Holmén, K., Berg, T., Schmidbauer, N., and Solberg, S.: Springtime depletion of tropospheric ozone, gaseous elemental mercury and non-methane hydrocarbons in the European Arctic, and its relation to atmospheric transport, Atmos. Environ., 41, 8511–8526, doi:10.1016/j.atmosenv.2007.07.008, 2007. 13836

Fahey, D. W., Eubank, C. S., Hubler, G., and Fehsenfeld, F. C.: Evaluation of a catalytic reduction technique for the measurement of total reactive odd-nitrogen NO_y in the atmosphere, Atmos. Chem., 3, 435–468, 1985. 13823

Ford, K. M., Campbell, B. M., Bertman, S. B., Honrath, R. E., Peterson, M. C., and Dibb, J. E.: Studies of Peroxyacetyl nitrate (PAN) and its interaction with the snowpack at Summit, Greenland, J. Geophys. Res., 107, 1–10, 2002. 13830, 13832

Gilman, J. B. B., Burkhart, J. F. J. F., Lerner, B. M., Williams, E. J., Kuster, W. C., Goldan, P. D., Murphy, P. C., Warneke, C., Fowler, C., Montzka, S. A., Miller, B. R., Miller, L., Oltmans, S. J.,

ACPD
14, 13817–13867, 2014

Seasonal variability of nitrogen oxides and NMHC at Summit

L. J. Kramer

Title Page
Abstract Introduction
Conclusions References
Tables Figures
◂ ▸
Back Close
Full Screen / Esc
Printer-friendly Version
Interactive Discussion

Ryerson, T. B., Cooper, O. R., Stohl, A., and de Gouw, J. A.: Ozone variability and halogen oxidation within the Arctic and sub-Arctic springtime boundary layer, Atmos. Chem. Phys., 10, 15885–15919, doi:10.5194/acpd-10-15885-2010, 2010. 13822

Grannas, A. M., Jones, A. E., Dibb, J., Ammann, M., Anastasio, C., Beine, H. J., Bergin, M., Bottenheim, J., Boxe, C. S., Carver, G., Chen, G., Crawford, J. H., Dominé, F., Frey, M. M., Guzmán, M. I., Heard, D. E., Helmig, D., Hoffmann, M. R., Honrath, R. E., Huey, L. G., Hutterli, M., Jacobi, H. W., Klán, P., Lefer, B., McConnell, J., Plane, J., Sander, R., Savarino, J., Shepson, P. B., Simpson, W. R., Sodeau, J. R., von Glasow, R., Weller, R., Wolff, E. W., and Zhu, T.: An overview of snow photochemistry: evidence, mechanisms and impacts, Atmos. Chem. Phys., 7, 4329–4373, doi:10.5194/acp-7-4329-2007, 2007. 13832, 13844

Hamlin, A. and Honrath, R.: A modeling study of the impact of winter-spring arctic outflow on the NO_x and O_3 budgets of the North Atlantic troposphere, J. Geophys. Res., 107, 1–46, doi:10.1029/2001JD000453, 2002. 13822, 13842, 13844

Helmig, D., Oltmans, S. J., Carlson, D., Lamarque, J.-F., Jones, A., Labuschagne, C., Anlauf, K., and Hayden, K.: A review of surface ozone in the polar regions, Atmos. Environ., 41, 5138–5161, doi:10.1016/j.atmosenv.2006.09.053, 2007a. 13843

Helmig, D., Oltmans, S. J., Morse, T. O., and Dibb, J. E.: What is causing high ozone at Summit, Greenland?, Atmos. Environ., 41, 5031–5043, doi:10.1016/j.atmosenv.2006.05.084, 2007b. 13821, 13843

Helmig, D., Tanner, D. M., Honrath, R. E., Owen, R. C., and Parrish, D. D.: Nonmethane hydrocarbons at Pico Mountain, Azores: 1. Oxidation chemistry in the North Atlantic region, J. Geophys. Res., 113, D20S91, doi:10.1029/2007JD008930, 2008. 13837

Helmig, D., Stephens, C., Caramore, J., and Hueber, J.: Seasonal behavior of non-methane hydrocarbons in the firn air at Summit, Greenland, Atmos. Environ., 85, 234–246, doi:10.1016/j.atmosenv.2013.11.021, 2014a. 13821, 13827, 13833

Helmig, D., Petrenko, V., Martinerie, P., Witrant, E., Röckmann, T., Zuiderweg, A., Holzinger, R., Hueber, J., Thompson, C., White, J. W. C., Sturges, W., Baker, A., Blunier, T., Etheridge, D., Rubino, M., and Tans, P.: Reconstruction of Northern Hemisphere 1950–2010 atmospheric non-methane hydrocarbons, Atmos. Chem. Phys., 14, 1463–1483, doi:10.5194/acp-14-1463-2014, 2014b. 13833

Hirdman, D., Sodemann, H., Eckhardt, S., Burkhart, J. F., Jefferson, A., Mefford, T., Quinn, P. K., Sharma, S., Ström, J., and Stohl, A.: Source identification of short-lived air pollutants in the

Arctic using statistical analysis of measurement data and particle dispersion model output, Atmos. Chem. Phys., 10, 669–693, doi:10.5194/acp-10-669-2010, 2010. 13836, 13843
Honrath, R. E. and Jaffe, D. A.: The seasonal cycle of nitrogen oxides in the Arctic troposphere at Barrow, Alaska, J. Geophys. Res., 97, 20615, doi:10.1029/92JD02081, 1992. 13821
Honrath, R., Hamlin, A., and Merrill, J.: Transport of ozone precursors from the Arctic troposphere to the North Atlantic region, J. Geophys. Res., 101, 29335–29351, 1996. 13822, 13833
Honrath, R., Peterson, M., Guo, S., Dibb, J. E., Shepson, P. B., and Campbell, B.: Evidence of NO_x production within or upon ice particles in the Greenland snowpack, Geophys. Res. Lett., 26, 695–698, 1999. 13830, 13832
Honrath, R. E., Guo, S., and Peterson, M. C.: Photochemical production of gas phase NO from ice crystal NO_3^-, J. Geophys. Res., 105, 24183–24190, 2000a. 13832
Honrath, R. E., Peterson, M. C., Dziobak, M. P., Dibb, J. E., Arsenault, M. A., and Green, S. A.: Release of NO_x from sunlight-irradiated midlatitude snow, Geophys. Res. Lett., 27, 2237–2240, doi:10.1029/1999GL011286, 2000b. 13832
Honrath, R. E., Lu, Y., and Peterson, M. C.: Vertical fluxes of NO_x, HONO, and HNO_3 above the snowpack at Summit, Greenland, Atmos. Environ., 36, 2629–2640, 2002. 13832
Honrath, R. E., Helmig, D., Owen, R. C., Parrish, D. D., and Tanner, D. M.: Nonmethane hydrocarbons at Pico Mountain, Azores: 2. Event-specific analyses of the impacts of mixing and photochemistry on hydrocarbon ratios, J. Geophys. Res., 113, D20S92, doi:10.1029/2008JD009832, 2008. 13837
Hornbrook, R. S., Blake, D. R., Diskin, G. S., Fried, A., Fuelberg, H. E., Meinardi, S., Mikoviny, T., Richter, D., Sachse, G. W., Vay, S. A., Walega, J., Weibring, P., Weinheimer, A. J., Wiedinmyer, C., Wisthaler, A., Hills, A., Riemer, D. D., and Apel, E. C.: Observations of nonmethane organic compounds during ARCTAS – Part 1: Biomass burning emissions and plume enhancements, Atmos. Chem. Phys., 11, 11103–11130, doi:10.5194/acp-11-11103-2011, 2011. 13839
Jobson, B., Wu, Z., Niki, H., and Barrie, L. A.: Seasonal trends of isoprene, C_2–C_5 alkanes, and acetylene at a remote boreal site in Canada, J. Geophys. Res., 99, 1589–1599, 1994. 13821
Karbiwnyk, C. M., Mills, C. S., Helmig, D., and Birks, J. W.: Use of chloroflurocarbons as internal standards for the measurement of atmospheric non-methane volatile organic compounds sampled onto solid adsorbent cartridges, Environ. Sci. Technol., 37, 1002–7, 2003. 13826

Kley, D. and Mcfarland, M.: Chemiluminescence detector for NO and NO_2, Atmospheric Measurement Techniques, 12, 63–69, 1980. 13823
Klonecki, A., Hess, P., Emmons, L., Smith, L., Orlando, J, and Blake, D.: Seasonal changes in the transport of pollutants into the Arctic troposphere-model study, J. Geophys. Res., 108, 8367, doi:10.1029/2002JD002199, 2003. 13820, 13821
Lapina, K., Honrath, R. E., Owen, R. C., Val Martín, M., Hyer, E. J., and Fialho, P.: Late summer changes in burning conditions in the boreal regions and their implications for NO_x and CO emissions from boreal fires, J. Geophys. Res., 113, D11304, doi:10.1029/2007JD009421, 2008. 13839
Law, K. S. and Stohl, A.: Arctic air pollution: origins and impacts, Science, 315, 1537–1540, doi:10.1126/science.1137695, 2007. 13820, 13821
Liang, Q., Rodriguez, J. M., Douglass, A. R., Crawford, J. H., Olson, J. R., Apel, E., Bian, H., Blake, D. R., Brune, W., Chin, M., Colarco, P. R., da Silva, A., Diskin, G. S., Duncan, B. N., Huey, L. G., Knapp, D. J., Montzka, D. D., Nielsen, J. E., Pawson, S., Riemer, D. D., Weinheimer, A. J., and Wisthaler, A.: Reactive nitrogen, ozone and ozone production in the Arctic troposphere and the impact of stratosphere-troposphere exchange, Atmos. Chem. Phys., 11, 13181–13199, doi:10.5194/acp-11-13181-2011, 2011. 13820, 13822, 13829, 13830, 13832, 13839
Monks, P. S.: A review of the observations and origins of the spring ozone maximum, Atmos. Environ., 34, 3545–3561, doi:10.1016/S1352-2310(00)00129-1, 2000. 13821, 13833
Moxim, W., Levy II, H., and Kasibhatla, P. S.: Simulated global tropospheric PAN: Its transport and impact on NO_x, J. Geophys. Res., 101, 12621–12638, 1996. 13836
Munger, J. W., Jacob, D. J., and Fan, S. M., Colman, A. S., and Dibb, J. E.: Concentrations and snow-atmosphere fluxes of reactive nitrogen at Summit, Greenland, J. Geophys. Res., 104, 13,721–13,734, 1999. 13821, 13830, 13832
Muthuramu, K., Shepson, P. B., Bottenheim, J. W., Jobson, B. T., Niki, H., and Anlauf, K. G.: Relationships between organic nitrates and surface ozone destruction during Polar Sunrise Experiment 1992, J. Geophys. Res., 99, 13,721–13,734, 1994. 13821
Parrish, D. D.Parrish, Dunlea, E. J., Atlas, E. L., Schauffler, S., Donnelly, S., Stoud, V., Goldstein, A. H., Millet, D. B., McKay, M., Jaffe, D. A., Price, H. U., Hess, P. G., Flocke, F., and Roberts, J. M: Changes in the photochemical environment of the temperate North Pacific troposphere in response to increased Asian emissions, J. Geophys. Res., 109, D23S18, doi:10.1029/2004JD004978, 2004. 13837

ACPD
14, 13817–13867, 2014

Penkett, S., Blake, N., Lightman, P., Marsh, A., Anwyl, P., and Butcher, G.: The seasonal variation of nonmethane hydrocarbons in the free troposphere over the North Atlantic Ocean: possible evidence for extensive reaction of hydrocarbons, J. Geophys. Res., 98, 2865–2885, 1993. 13833

Peterson, M. C. and Honrath, R. E.: NO_x and NO_y over the northwestern North Atlantic: measurements and measurement accuray, J. Geophys. Res., 103, 13489–13503, 1999. 13823

Petropavlovskikh, I. and Oltmans, S. J.: Tropospheric Ozone Measurements, 1973–2011, Version: 2012-07-10, NOAA, ftp://aftp.cmdl.noaa.gov/data/ozwv/SurfaceOzone/ (last access: 24 March 2013), 2012 13828

Pollack, I. B., Lerner, B. M., and Ryerson, T. B.: Evaluation of ultraviolet light-emitting diodes for detection of atmospheric NO_2 by photolysis – chemiluminescence, J. Atmos. Chem., 65, 111–125, doi:10.1007/s10874-011-9184-3, 2011. 13823

Quennehen, B., Schwarzenboeck, A., Schmale, J., Schneider, J., Sodemann, H., Stohl, A., Ancellet, G., Crumeyrolle, S., and Law, K. S.: Physical and chemical properties of pollution aerosol particles transported from North America to Greenland as measured during the POLARCAT summer campaign, Atmos. Chem. Phys., 11, 10947–10963, doi:10.5194/acp-11-10947-2011, 2011. 13839

Quennehen, B., Schwarzenboeck, A., Matsuki, A., Burkhart, J. F., Stohl, A., Ancellet, G., and Law, K. S.: Anthropogenic and forest fire pollution aerosol transported to the Arctic: observations from the POLARCAT-France spring campaign, Atmos. Chem. Phys., 12, 6437–6454, doi:10.5194/acp-12-6437-2012, 2012. 13839

Quinn, P. K., Bates, T. S., Baum, E., Doubleday, N., Fiore, A. M., Flanner, M., Fridlind, A., Garrett, T. J., Koch, D., Menon, S., Shindell, D., Stohl, A., and Warren, S. G.: Short-lived pollutants in the Arctic: their climate impact and possible mitigation strategies, Atmos. Chem. Phys., 8, 1723–1735, doi:10.5194/acp-8-1723-2008, 2008. 13820

Ridley, B. A. and Grahek, F.: A small, low flow, high sensitivity reaction vessel for NO chemiluminescence detectors, American Meteorlogical Society, 7, 307–311, 1990. 13823

Roiger, A., Aufmhoff, H., Stock, P., Arnold, F., and Schlager, H.: An aircraft-borne chemical ionization – ion trap mass spectrometer (CI-ITMS) for fast PAN and PPN measurements, Atmos. Meas. Tech., 4, 173–188, doi:10.5194/amt-4-173-2011, 2011. 13841

Schmale, J., Schneider, J., Ancellet, G., Quennehen, B., Stohl, A., Sodemann, H., Burkhart, J. F., Hamburger, T., Arnold, S. R., Schwarzenboeck, A., Borrmann, S., and Law, K. S.: Source identification and airborne chemical characterisation of aerosol pollution

ACPD
14, 13817–13867, 2014

Seasonal variability of nitrogen oxides and NMHC at Summit

L. J. Kramer

from long-range transport over Greenland during POLARCAT summer campaign 2008, Atmos. Chem. Phys., 11, 10097–10123, doi:10.5194/acp-11-10097-2011, 2011. 13839
Shindell, D.: Local and remote contributions to Arctic warming, Geophys. Res. Lett., 34, L14704, doi:10.1029/2007GL030221, 2007. 13820
Shindell, D., Faluvegi, G., Lacis, A., Hansen, J., Ruedy, R., and Aguilar, E.: Role of tropospheric ozone increases in 20th-century climate change, J. Geophys. Res., 111, D08302, doi:10.1029/2005JD006348, 2006. 13820
Shindell, D. T., Chin, M., Dentener, F., Doherty, R. M., Faluvegi, G., Fiore, A. M., Hess, P., Koch, D. M., MacKenzie, I. A., Sanderson, M. G., Schultz, M. G., Schulz, M., Stevenson, D. S., Teich, H., Textor, C., Wild, O., Bergmann, D. J., Bey, I., Bian, H., Cuvelier, C., Duncan, B. N., Folberth, G., Horowitz, L. W., Jonson, J., Kaminski, J. W., Marmer, E., Park, R., Pringle, K. J., Schroeder, S., Szopa, S., Takemura, T., Zeng, G., Keating, T. J., and Zuber, A.: A multi-model assessment of pollution transport to the Arctic, Atmos. Chem. Phys., 8, 5353–5372, doi:10.5194/acp-8-5353-2008, 2008. 13821
Singh, H., Anderson, B., Brune, W., Cai, C., Cohen, R., Crawford, J., Cubison, M., Czech, E., Emmons, L., and Fuelberg, H.: Pollution influences on atmospheric composition and chemistry at high northern latitudes: boreal and California forest fire emissions, Atmos. Environ., 44, 4553–4564, doi:10.1016/j.atmosenv.2010.08.026, 2010. 13830, 13839
Solberg, S., Krognes, T., Stordal, F., Hov, Ø., Beine, H. J., Jaffe, D. A., Clemitshaw, K. C., and Penkett, S. A.: Reactive nitrogen compounds at Spitsbergen in the Norwegian Arctic, J. Atmos. Chem., 28, 209–225, 1997. 13821, 13830, 13831
Stohl, A.: Characteristics of atmospheric transport into the Arctic troposphere, J. Geophys. Res., 111, D11306, doi:10.1029/2005JD006888, 2006. 13821, 13830, 13839
Stohl, A., Forster, C., Eckhardt, S., Spichtinger, N., Huntrieser, H., Heland, J., Schlager, H., Wilhelm, S., Arnold, F., and Cooper, O.: A backward modeling study of intercontinental pollution transport using aircraft measurements, J. Geophys. Res., 108, 4370, doi:10.1029/2002JD002862, 2003. 13828
Stohl, A., Forster, C., Frank, A., Seibert, P., and Wotawa, G.: Technical note: The Lagrangian particle dispersion model FLEXPART version 6.2, Atmos. Chem. Phys., 5, 2461–2474, doi:10.5194/acp-5-2461-2005, 2005. 13828
Stohl, A., Andrews, E., Burkhart, J. F., Forster, C., Herber, A., Hoch, S. W., Kowal, D., Lunder, C., Mefford, T., Ogren, J. A., Sharma, S., Spichtinger, N., Stebel, K., Stone, R., Ström, J., Tørseth, K., Wehrli, C., and Yttri, K. E.: Pan-Arctic enhancements of light absorbing aerosol

ACPD
14, 13817–13867, 2014

Seasonal variability of nitrogen oxides and NMHC at Summit

L. J. Kramer

concentrations due to North American boreal forest fires during summer 2004, J. Geophys. Res., 111, D22214, doi:10.1029/2006JD007216, 2006. 13820, 13821, 13839
Stohl, A., Berg, T., Burkhart, J. F., Fjæraa, A. M., Forster, C., Herber, A., Hov, Ø., Lunder, C., McMillan, W. W., Oltmans, S., Shiobara, M., Simpson, D., Solberg, S., Stebel, K., Ström, J., Tørseth, K., Treffeisen, R., Virkkunen, K., and Yttri, K. E.: Arctic smoke – record high air pollution levels in the European Arctic due to agricultural fires in Eastern Europe in spring 2006, Atmos. Chem. Phys., 7, 511–534, doi:10.5194/acp-7-511-2007, 2007. 13839
Stohl, A., Klimont, Z., Eckhardt, S., Kupiainen, K., Shevchenko, V. P., Kopeikin, V. M., and Novigatsky, A. N.: Black carbon in the Arctic: the underestimated role of gas flaring and residential combustion emissions, Atmos. Chem. Phys., 13, 8833–8855, doi:10.5194/acp-13-8833-2013, 2013. 13829
Stroud, C., Madronich, S., Atlas, E., Ridley, B., Flocke, F., Weinheimer, A., Talbot, B., Fried, A., Wert, B., Shetter, R., Lefer, B., Coffey, M., Heikes, B., and Blake, D.: Photochemistry in the arctic free troposphere: NO_x budget and the role of odd nitrogen reservoir recycling, Atmos. Environ., 37, 3351–3364, doi:10.1016/S1352-2310(03)00353-4, 2003. 13821
Swanson, A. L., Blake, N. J., Atlas, E., Flocke, F., Blake, D. R., and Sherwood Rowland, F.: Seasonal variations of C_2–C_4 nonmethane hydrocarbons and C_1–C_4 alkyl nitrates at the Summit research station in Greenland, J. Geophys. Res., 108, 4065, doi:10.1029/2001JD001445, 2003. 13821, 13831, 13833
Tanner, D., Helmig, D., Hueber, J., and Goldan, P.: Gas chromatography system for the automated, unattended, and cryogen-free monitoring of C_2 to C_6 non-methane hydrocarbons in the remote troposphere, J. Chromatogr. A, 1111, 76–88, doi:10.1016/j.chroma.2006.01.100, 2006. 13827
Thomas, J. L., Stutz, J., Lefer, B., Huey, L. G., Toyota, K., Dibb, J. E., and von Glasow, R.: Modeling chemistry in and above snow at Summit, Greenland – Part 1: Model description and results, Atmos. Chem. Phys., 11, 4899–4914, doi:10.5194/acp-11-4899-2011, 2011. 13821
Thomas, J. L., Raut, J.-C., Law, K. S., Marelle, L., Ancellet, G., Ravetta, F., Fast, J. D., Pfister, G., Emmons, L. K., Diskin, G. S., Weinheimer, A., Roiger, A., and Schlager, H.: Pollution transport from North America to Greenland during summer 2008, Atmos. Chem. Phys., 13, 3825–3848, doi:10.5194/acp-13-3825-2013, 2013. 13840
Val Martín, M., Honrath, R. E., Owen, R. C., Pfister, G., Fialho, P., and Barata, F.: Significant enhancements of nitrogen oxides, black carbon, and ozone in the North Atlantic lower free

troposphere resulting from North American boreal wildfires, J. Geophys. Res., 111, 1–17, doi:10.1029/2006JD007530, 2006. 13823

Villena, G., Bejan, I., Kurtenbach, R., Wiesen, P., and Kleffmann, J.: Interferences of commercial NO_2 instruments in the urban atmosphere and in a smog chamber, Atmos. Meas. Tech., 5, 149–159, doi:10.5194/amt-5-149-2012, 2012. 13823

Walker, T. W., Martin, R. V., van Donkelaar, A., Leaitch, W. R., MacDonald, A. M., Anlauf, K. G., Cohen, R. C., Bertram, T. H., Huey, L. G., Avery, M. A., Weinheimer, A. J., Flocke, F. M., Tarasick, D. W., Thompson, A. M., Streets, D. G., and Liu, X.: Trans-Pacific transport of reactive nitrogen and ozone to Canada during spring, Atmos. Chem. Phys., 10, 8353–8372, doi:10.5194/acp-10-8353-2010, 2010. 13820

Walker, T. W., Jones, D. B. A., Parrington, M., Henze, D. K., Murray, L. T., Bottenheim, J. W., Anlauf, K., Worden, J. R., Bowman, K. W., Shim, C., Singh, K., Kopacz, M., Tarasick, D. W., Davies, J., von der Gathen, P., Thompson, A. M., and Carouge, C. C.: Impacts of midlatitude precursor emissions and local photochemistry on ozone abundances in the Arctic, J. Geophys. Res., 117, D01305, doi:10.1029/2011JD016370, 2012. 13821

Wang, Y. H., Ridley, B., Fried, A., Cantrell, C., Davis, D., Chen, G., Snow, J., Heikes, B., Talbot, R., Dibb, J., Flocke, F., Weinheimer, A., Blake, N., Blake, D., Shetter, R., Lefer, B., Atlas, E., Coffey, M., Walega, J., and Wert, B.: Springtime photochemistry at northern mid and high latitudes, J. Geophys. Res., 108, 8358, doi:10.1029/2002JD002227, 2003. 13833

Wespes, C., Emmons, L., Edwards, D. P., Hannigan, J., Hurtmans, D., Saunois, M., Coheur, P.-F., Clerbaux, C., Coffey, M. T., Batchelor, R. L., Lindenmaier, R., Strong, K., Weinheimer, A. J., Nowak, J. B., Ryerson, T. B., Crounse, J. D., and Wennberg, P. O.: Analysis of ozone and nitric acid in spring and summer Arctic pollution using aircraft, ground-based, satellite observations and MOZART-4 model: source attribution and partitioning, Atmos. Chem. Phys., 12, 237–259, doi:10.5194/acp-12-237-2012, 2012. 13820, 13821, 13832

Wofsy, S., Sachse, G., Gregory, G., Blake, D. R., Bradshaw, J. D., Sandholm, S. T., Singh, H., Barrick, J. A., Harriss, R. C., Talbot, R. W., Shipham, M. A., Browell, E. V., Jacob, D. J., and Logan, J. A.: Atmospheric chemistry in the Arctic and Subarctic: Influence of natural fires, industrial emissions, and stratospheric inputs, J. Geophys. Res., 97, 16731—16746, 1992. 13820

Worthy, D., Trivett, N., Hopper, J. F., Bottenheim, J. W., and Levin, I.: Analysis of long range transport events at Alert, Northwest Territories, during the Polar Sunrise Experiment, J. Geophys. Res., 25329–25344, 99, 1994. 13830

ACPD
14, 13817–13867, 2014

Seasonal variability of nitrogen oxides and NMHC at Summit

L. J. Kramer

Table 1. Monthly statistics for NO_x, NO_y, PAN and O_3 measured at Summit from 2008–2010.

	NO_x		NO_y		PAN		O_3	
Month	Mean ± SD (pmol mol^{-1})	Median (pmol mol^{-1})	Mean ± SD (pmol mol^{-1})	Median (pmol mol^{-1})	Mean ± SD (pmol mol^{-1})	Median (pmol mol^{-1})	Mean ± SD (nmol mol^{-1})	Median (nmol mol^{-1})
1	6 ± 11	3	181 ± 56	169	94 ± 30	84	45 ± 3	45
2	6 ± 12	3	243 ± 92	215	128 ± 61	111	47 ± 3	46
3	10 ± 10	9	246 ± 66	231	183 ± 79	159	50 ± 4	50
4	23 ± 19	19	321 ± 98	306	241 ± 77	235	54 ± 7	54
5	29 ± 24	24	257 ± 73	246	176 ± 40	166	55 ± 7	55
6	22 ± 14	20	171 ± 61	155	97 ± 32	96	48 ± 7	47
7	19 ± 16	16	160 ± 73	148	66 ± 29	65	46 ± 6	46
8	15 ± 12	13	141 ± 48	136	98 ± 39	96	44 ± 6	44
9	10 ± 11	8	100 ± 43	87	76 ± 35	69	41 ± 6	41
10	6 ± 10	4	132 ± 51	119	94 ± 35	88	41 ± 5	41
11	6 ± 12	3	172 ± 38	166	118 ± 33	112	42 ± 4	42
12	6 ± 14	3	179 ± 52	185	93 ± 31	85	43 ± 4	43

ACPD
14, 13817–13867, 2014

Table 2. Monthly statistics for NMHC measured at Summit from 2008–2010.

Month	Ethane ($pmol\,mol^{-1}$) Mean ± SD	Propane ($pmol\,mol^{-1}$) Mean ± SD	n-Butane ($pmol\,mol^{-1}$) Mean ± SD	i-Butane ($pmol\,mol^{-1}$) Mean ± SD	n-Pentane ($pmol\,mol^{-1}$) Mean ± SD	i-Pentane ($pmol\,mol^{-1}$) Mean ± SD
1	1780 ± 298	783 ± 197	281 ± 92	151 ± 47	77 ± 31	97 ± 41
2	1810 ± 254	735 ± 170	244 ± 77	133 ± 41	61 ± 24	75 ± 31
3	1970 ± 209	725 ± 174	215 ± 76	118 ± 41	47 ± 23	59 ± 30
4	1780 ± 232	482 ± 172	104 ± 73	61 ± 38	21 ± 17	25 ± 21
5	1350 ± 154	192 ± 66	27 ± 14	17 ± 9	6 ± 4	8 ± 7
6	897 ± 100	64 ± 24	8 ± 4	5 ± 5	4 ± 4	10 ± 16
7	660 ± 67	51 ± 22	9 ± 6	8 ± 5	5 ± 4	8 ± 8
8	633 ± 65	73 ± 19	15 ± 6	8 ± 4	4 ± 2	5 ± 3
9	683 ± 96	126 ± 35	34 ± 22	20 ± 12	11 ± 7	11 ± 7
10	908 ± 178	270 ± 105	87 ± 39	44 ± 19	25 ± 12	29 ± 17
11	1280 ± 160	490 ± 112	162 ± 47	88 ± 27	46 ± 19	57 ± 22
12	1510 ± 198	652 ± 147	225 ± 76	122 ± 37	62 ± 24	79 ± 29

ACPD
14, 13817–13867, 2014

Table 3. Mean enhancements in trace gases measured at Summit during biomass burning events.

Event	Start Date	Event Length (h)	BC_{fire} (pmol mol^{-1})	ΔO_3[a] (nmol mol^{-1})	ΔPAN (pmol mol^{-1})	ΔNO_x (pmol mol^{-1})	ΔNO_y (pmol mol^{-1})	ΔC_2H_6 (pmol mol^{-1})	Plume age[b] (days)	Source[c]	BC_{anthro}[d]
1	25 Jun 2008	33	30.6	−3.6	−4.2	0.6	−5.6	34.4	9	NA	med
2	1 Aug 2008	15	25.0	7.0	−6.3	6.3	20.6	–	15	NA	low
3	3 Aug 2008	252	90.7	10.5	56.5	19.4	141.1	–	14	NA	med
4	15 Mar 2009	60	58.6	−0.7	5.3	–	–	338.0	12	EU	med
5	18 Mar 2009	33	23.1	3.6	13.1	–	–	220.3	15	EU	med
6	21 Mar 2009	21	17.6	3.6	−7.9	–	–	243.1	16	EU	low
7	27 May 2009	30	17.7	12.4	67.9	–	–	–	16	AS	med
8	17 Jul 2009	12	19.9	2.4	90.4	6.3	105.1	−22.9	13	NA	low
9	18 Jul 2009	15	13.5	10.8	74.9	24.5	126.5	12.0	14	NA	low
10	16 Aug 2009	18	11.8	−4.4	5.1	14.1	22.1	–	18	NA	low
11	18 Aug 2009	12	9.5	5.6	79.5	2.6	71.0	113.0	17	NA	med
12	7 Jun 2010	27	11.3	7.5	–	14.9	122.8	60.7	13	NA	high
13	18 Jul 2010	51	27.4	9.5	–	12.2	184.8	118.3	9	NA	high

[a] Δ represents the enhancement over the background level (background = 20th percentile of each species for each month);
[b] Mean weighted age from FLEXPART.
[c] Primary BB source. NA = North America, EU = Europe, AS = Asia;
[d] Indicates potential contribution from anthropogenic pollution. Low: BC_{anthro} < 50th percentile, Med: BC_{anthro}, < 75th percentile, high: BC_{anthro}, > 75th percentile

ACPD
14, 13817–13867, 2014

ACPD
14, 13817–13867, 2014

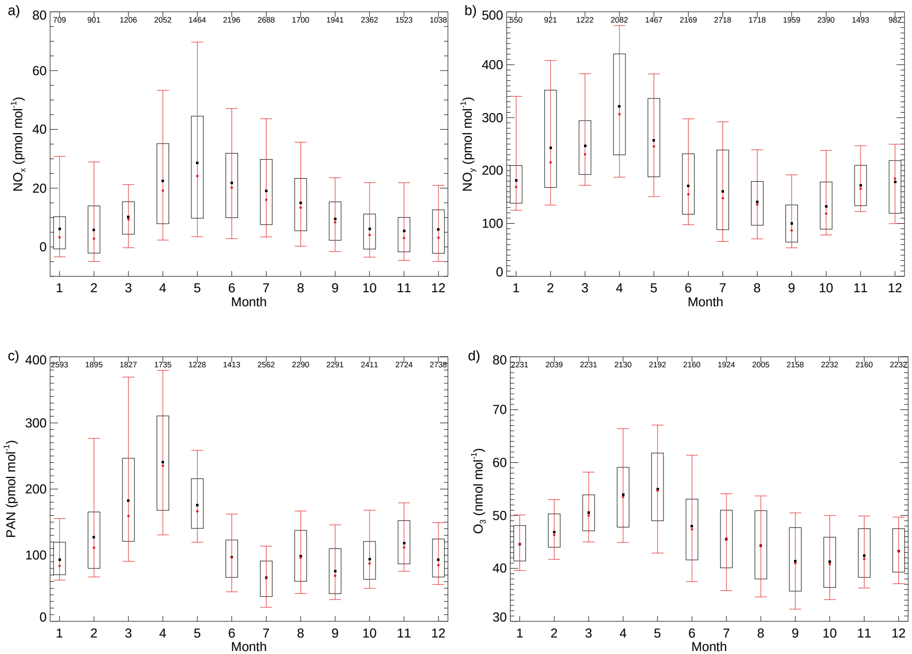

Figure 1. Seasonal cycle of **(a)** NO_x, **(b)** NO_y, **(c)** PAN and **(d)** O_3 at Summit during 2008–2010. The median and mean are indicated by a filled red circle and black square, respectively; the box indicates the middle 67 % of the data; and the top and bottom of the vertical whiskers indicate the 1st and 99th percentile of all the data. The numbers at the top of each plot represent the number of 30 min averages included in the distribution.

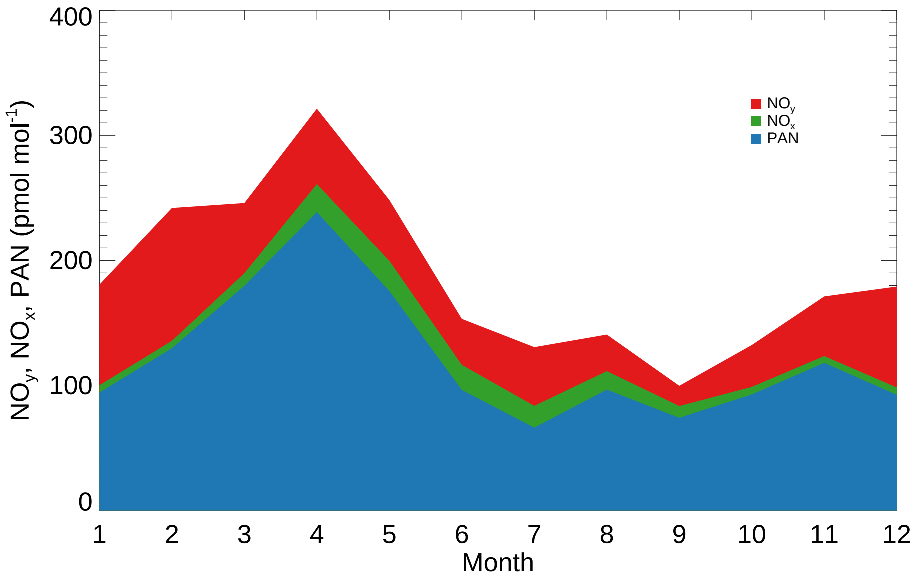

Figure 2. Monthly average contribution of PAN (Blue) and NO_x (Green) to NO_y (Red) for 2008–2010 at Summit. Only coincident data are considered in this analysis.

ACPD
14, 13817–13867, 2014

Seasonal variability of nitrogen oxides and NMHC at Summit

L. J. Kramer

Title Page
Abstract Introduction
Conclusions References
Tables Figures
Back Close
Full Screen / Esc
Printer-friendly Version
Interactive Discussion

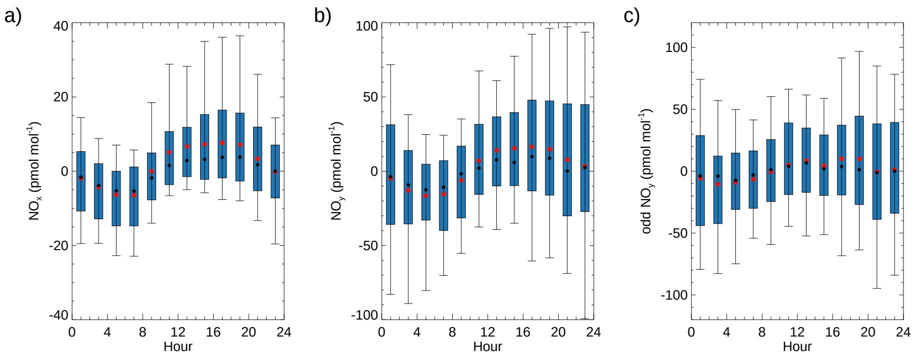

Figure 3. Average diurnal cycle of ambient **(a)** NO_x, **(b)** NO_y and **(c)** odd NO_y measured at Summit for the months April–June 2008–2010. Median ambient levels observed each day have been subtracted, to remove any impact from day to day variability. The median and mean of the data are represented by a filled black circle and red box, respectively; the blue box indicates the middle 67 % of the data; and the vertical whiskers indicate the middle 95 % of the data. Times are shown as local time (UTC – 2 h).

ACPD
14, 13817–13867, 2014

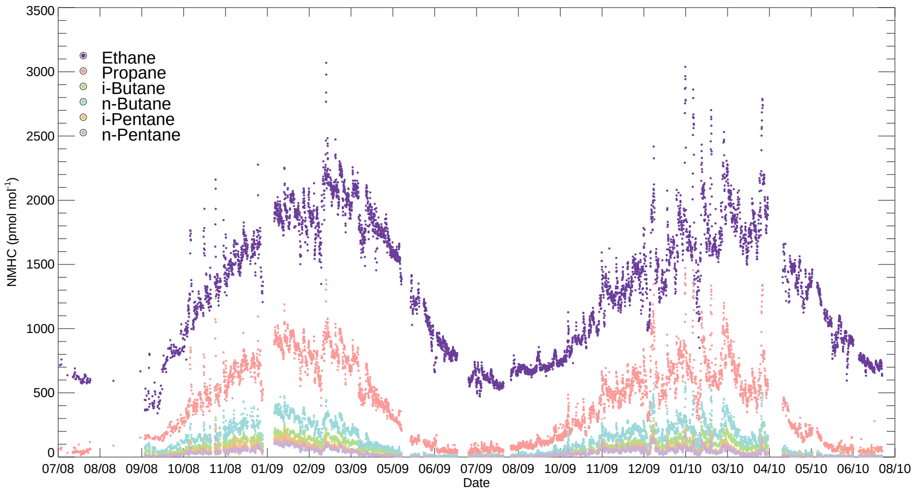

Figure 4. Seasonal cycle of NMHC mole fractions at Summit during 2008–2010.

ACPD
14, 13817–13867, 2014

Seasonal variability of nitrogen oxides and NMHC at Summit

L. J. Kramer

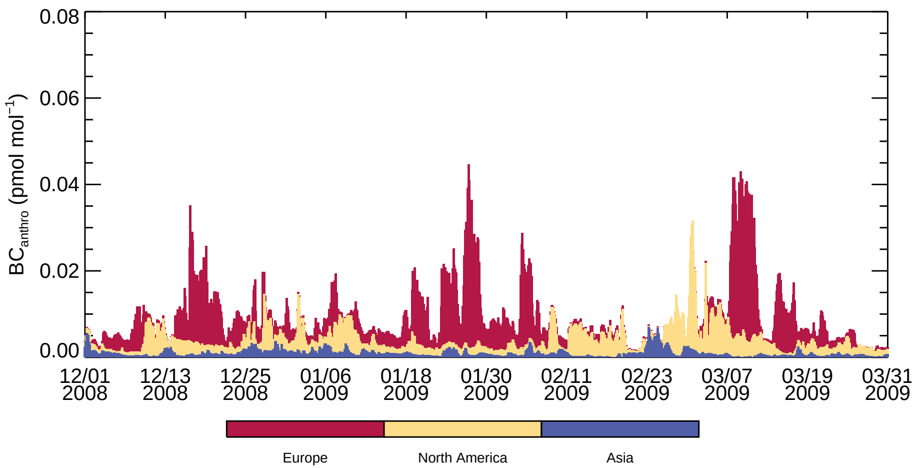

Figure 5. Stacked bar chart showing the source contribution to the FLEXPART anthropogenic BC tracer simulations at Summit for December 2008 to March 2009. The colors represent the BC anthropogenic tracer contribution from each region as shown in the legend.

ACPD
14, 13817–13867, 2014

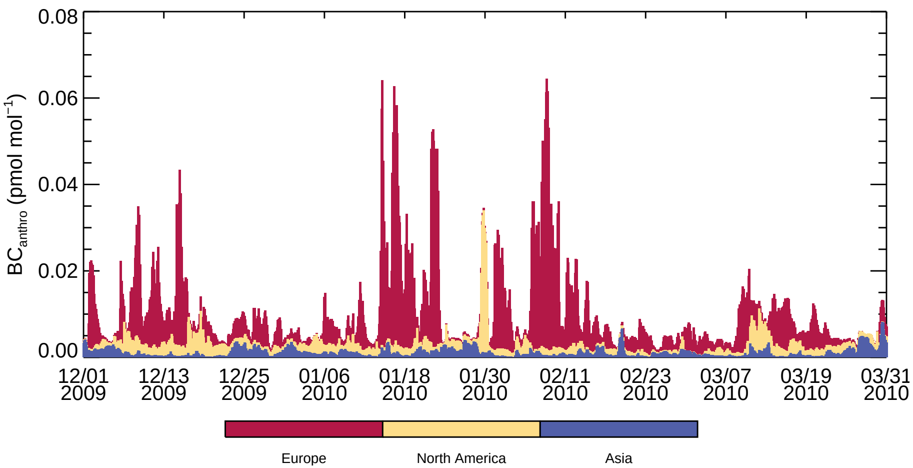

Figure 6. Same as Fig. 5 for December 2009 to March 2010.

ACPD
14, 13817–13867, 2014

Seasonal variability of nitrogen oxides and NMHC at Summit

L. J. Kramer

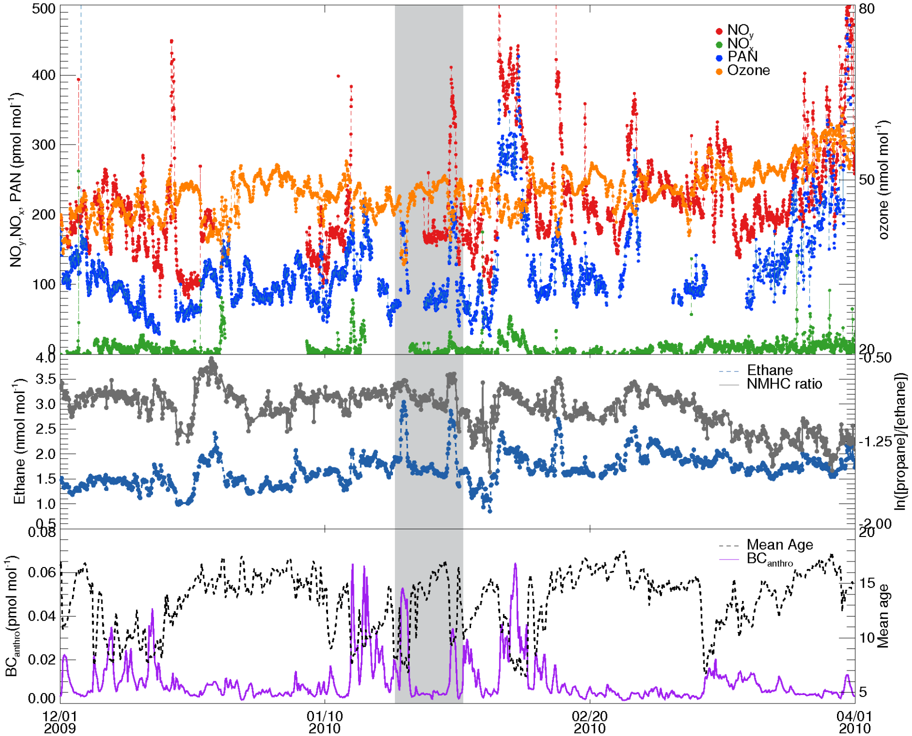

Figure 7. The top plot shows 30 min averages of NO_x, NO_y, PAN and 1 h average of O_3 from Summit between December 2009 and March 2010. The middle plot shows ethane mole fraction and ln([propane]/[ethane]) and the bottom plot shows the FLEXPART BC_{anthro} tracer emissions (from all continents), and mean weighted age, for the same period. The shaded area indicates the period discussed in detail in the main text.

ACPD
14, 13817–13867, 2014

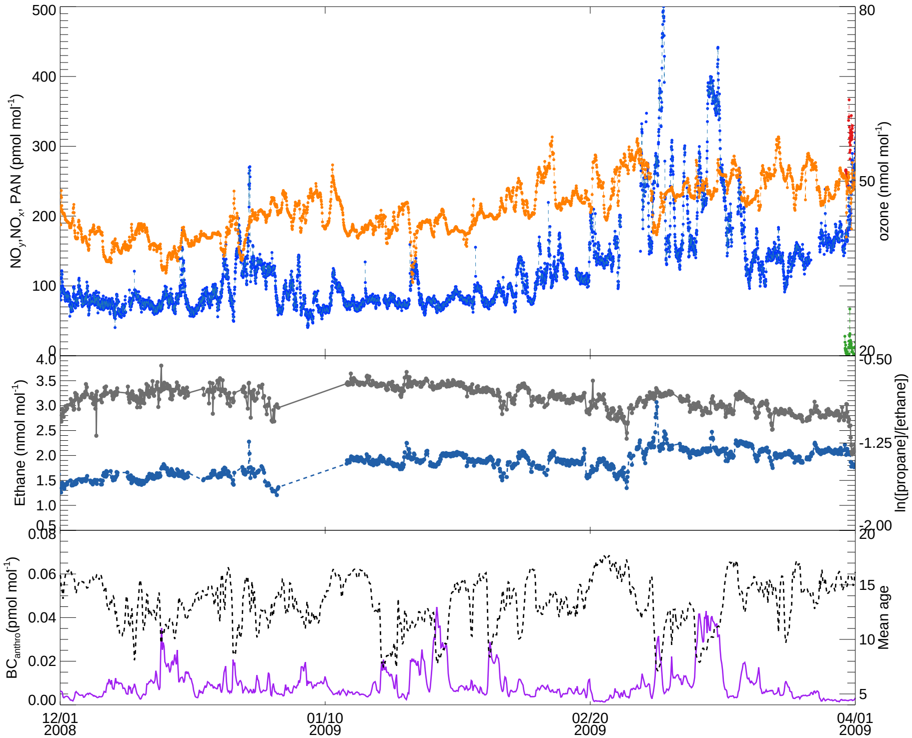

Figure 8. The same plot as Fig. 7 for the period December 2008 to March 2009.

ACPD
14, 13817–13867, 2014

Seasonal variability of nitrogen oxides and NMHC at Summit

L. J. Kramer

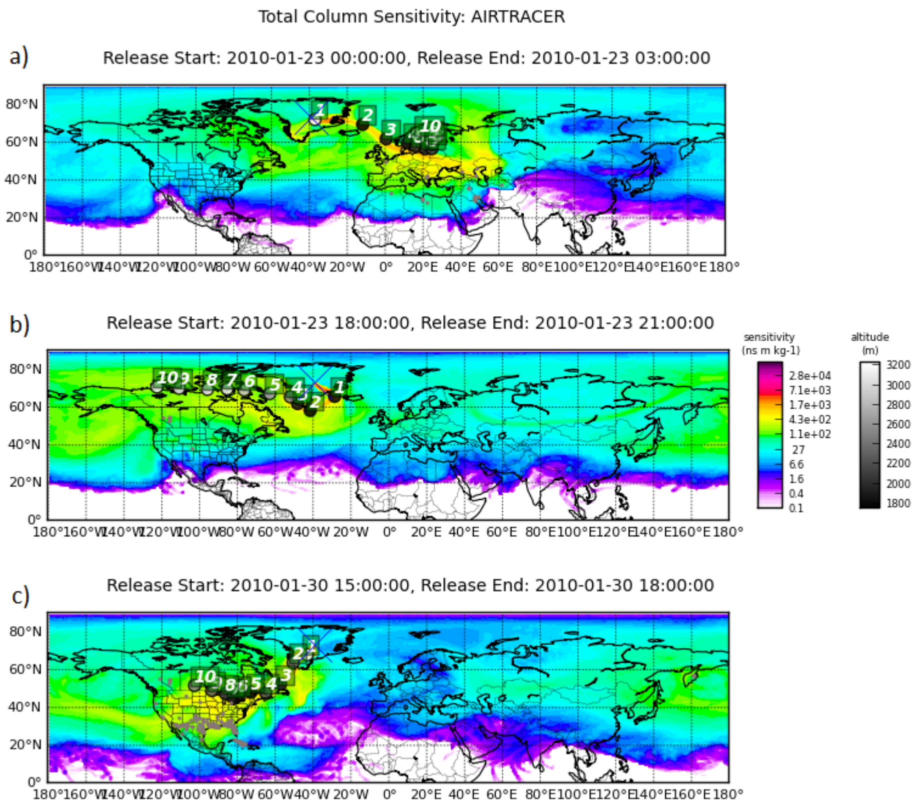

Figure 9. Simulated total column sensitivity (ns m kg^{-1}) for retroplumes originating at Summit on **(a)** 23 January 2010 at 00:00 UTC, **(b)** 23 January 2010 at 18:00 UTC and **(c)** 30 January 2010 at 15:00 UTC. The shaded circles are indicative of the approximate position and altitude (grey-shading) where the air resided up to 10 days (numbered labels) upwind of Summit (further information given in the main text).

ACPD
14, 13817–13867, 2014

Seasonal variability of nitrogen oxides and NMHC at Summit

L. J. Kramer

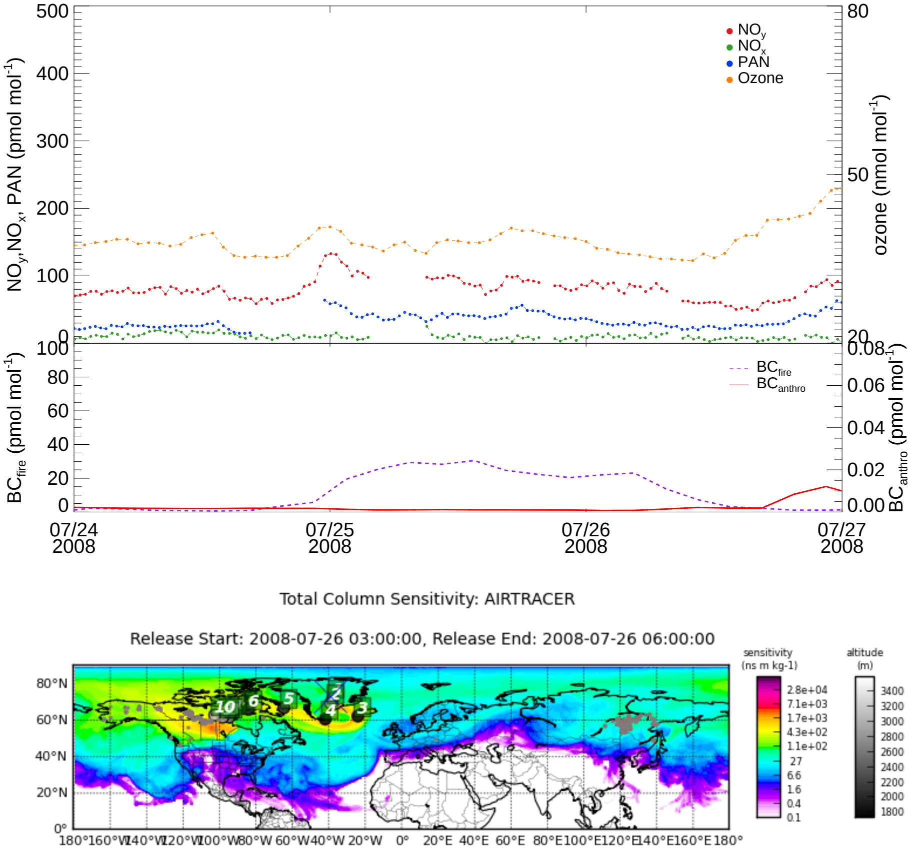

Figure 10. Top panel: 30 min averages of NO_x, NO_y, PAN and 1 h average of O_3 and FLEXPART BC_{fire} and BC_{anthro} tracer at Summit from 24–27 July 2008. Bottom panel: FLEXPART simulated total column sensitivity for retroplumes originating at Summit on 26 July 2008 at 03:00 UTC.

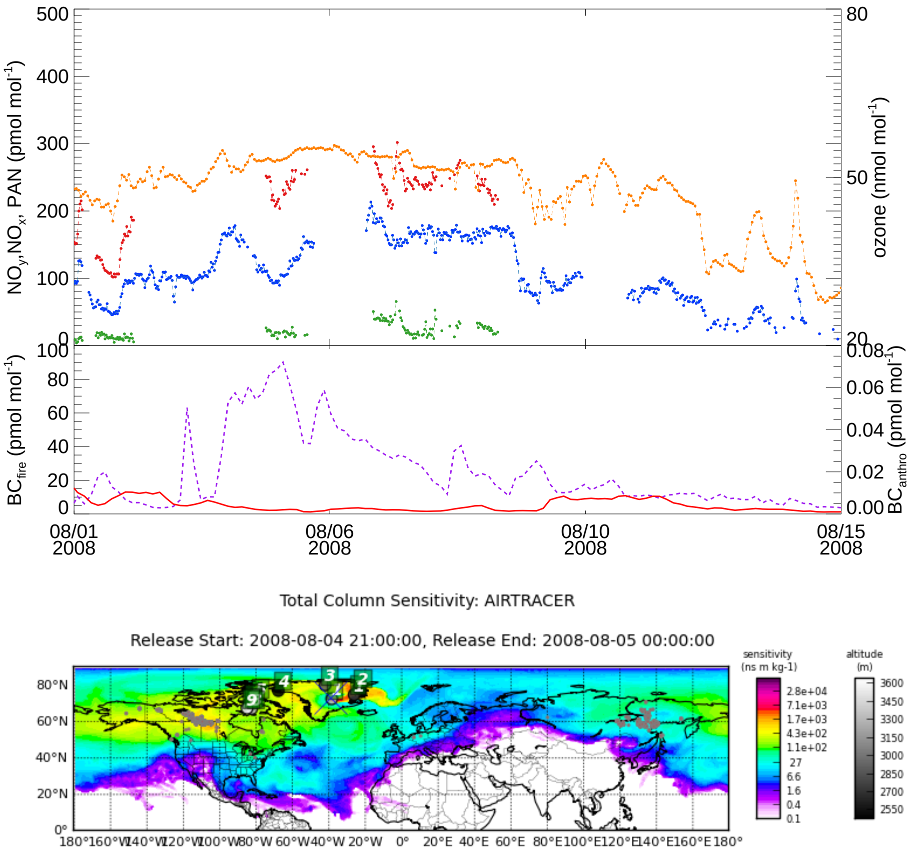

Figure 11. Top panel: 30 min averages of NO_x, NO_y, PAN and 1 h average of O_3 and FLEXPART BC_{fire} and BC_{anthro} tracer at Summit from 1–15 August 2008. Bottom panel: FLEXPART simulated total column sensitivity for retroplumes originating at Summit on 04 August 2008 at 21:00 UTC.

ACPD
14, 13817–13867, 2014

Seasonal variability of nitrogen oxides and NMHC at Summit

L. J. Kramer